IEEE Access
Multidisciplinary | Rapid Review | Open Access Journal

Received October 10, 2020, accepted October 25, 2020, date of publication October 29, 2020, date of current version November 12, 2020.

Digital Object Identifier 10.1109/ACCESS.2020.3034597

Optimization Analysis of Structural Parameters for Ball Screw Precision Retention Based on Advanced Neural Fuzzy Network

BAOBAO QI[1,2], QIANG CHENG[1,2], ZHIFENG LIU[1,3], AND CONGBIN YANG[1,3]

[1]Institute of Advanced Manufacturing and Intelligent Technology, Beijing University of Technology, Beijing 100124, China
[2]Beijing Key Laboratory of Advanced Manufacturing Technology, Beijing University of Technology, Beijing 100124, China
[3]Mechanical Industry Key Laboratory of Heavy Machine Tool Digital Design and Testing, Beijing University of Technology, Beijing 100124, China

Corresponding author: Qiang Cheng (chengqiangbjut@126.com)

This work was supported in part by the National Natural Science Foundation of China under Grant 51975012, in part by the Beijing Nova Programme Interdisciplinary Cooperation Project under Grant Z191100001119010, and in part by the National Science and Technology Major Project under Grant 2018ZX04033001-003.

ABSTRACT Ball screws are used as precision transmission components in a wide range of industries. The combination of sliding/rolling motion can influence the degree of precision degradation of the ball screw. Optimization analysis of structural parameters can reduce precision loss and improve precision retention. This article presents an optimization analysis of the ball screw to improve precision retention under mixed sliding-rolling motion. Precision loss of the ball screw due to mixed sliding-rolling motion was calculated. In addition, the effects of operating conditions and structural parameters on the precision loss were analyzed. Factors affecting precision loss of the ball screw under mixed motion were determined and the objective function to characterize precision retention was established according to imposed constraints. Structural parameter optimization of the ball screw based on an advanced neural fuzzy network can reduce the average rate of precision loss by approximately 18.36% and improve precision retention.

INDEX TERMS Ball screw, precision retention, structural parameters, optimization analysis, advanced neural fuzzy network.

NOMENCLATURE

a_n, b_n	contact long/short axis between ball and nut
a_{nLi}, b_{nLi}	contact long/short half axis between i-th ball and nut
a_{nRi}, b_{nRi}	contact long/short axis between No. i ball and nut
a_s, b_s	contact long/short axis between ball and screw
a_{sLi}, b_{sLi}	contact long/short half axis between No. i ball and screw
a_{sRi}, b_{sRi}	contact long/short axis between No. i ball and screw
$2a_{xn}, 2a_{yn}$	contact length of ball and nut in x_n/y_n direction
$2a_{xs}, 2a_{ys}$	contact length of ball and screw in x_s/y_s direction
A_n, A_s	nominal contact area between ball and nut/screw
A_{rn}, A_{rs}	actual contact area between ball and nut/screw
$A_{xn}, C_{xn}, A_{yn}, C_{yn}$	rolling contact point in x_n/y_n direction
$A_{xs}, C_{xs}, A_{ys}, C_{ys}$	rolling contact point in x_s/y_s direction
B_{xn}, B_{yn}	critical point of sliding and sticking in x_n/y_n direction
B_{xs}, B_{ys}	critical point of sliding and sticking in x_s/y_s direction
$2c_{xn}, 2c_{yn}$	creep length of ball and nut in x_n/y_n direction
$2c_{xs}, 2c_{ys}$	creep length of ball and screw in x_s/y_s direction
C_{b-s}, C_{b-n}	cycle number of ball relative to screw/nut raceway
$d_b^{xn}, d_b^{yn}, d_n^{xn}, d_n^{yn}$	ball/screw displacement in x_n/y_n direction

The associate editor coordinating the review of this manuscript and approving it for publication was Zheng Chen.

$d_b^{xs}, d_b^{ys}, d_s^{xs}, d_s^{ys}$	ball/screw displacement in x_s/y_s direction
D	nominal diameter of screw
D_b	ball diameter
D_f	fractal parameter
$h_{rbs}^{xn}, h_{rbs}^{yn}$	rolling wear depth between ball and nut in x_n/y_n direction
$h_{rbs}^{xs}, h_{rbs}^{ys}$	rolling wear depth between ball and screw in x_s/y_s direction
H_{b-s}, H_{b-n}	screw/nut hardness
H_{sbs}, H_{sbn}	precision loss between ball and screw/nut due to sliding wear
$H_{rbn}^{xn}, H_{rbn}^{yn}$	precision loss due to rolling wear in x_n/y_n direction
$H_{rbs}^{xs}, H_{rbs}^{ys}$	precision loss due to rolling wear in x_s/y_s direction
k_{bn}, k_{bs}	boundary wear coefficient
L_{bsi}, L_{bni}	sliding distance of screw/nut relative to No. i ball
L_{b-s}, L_{b-n}	the length of the screw/nut raceway as well as the abraded areas
L_s, L_n	effective travel of screw/nut
L_{SN}	distance of curvature center between screw raceway and nut raceway
M	number of balls in left/right nut
M_{bL}	number of balls in left nut
M_{bR}	number of balls in right nut
$n_{xs}, n_{ys}, n_{xn}, n_{yn}$	total number of rolling contact between ball and screw/nut
N_H	Hertz contact area parameter
$N_{L1}, S_{L1}, N_{R1}, S_{R1}$	initial contact center between ball and raceway
$N'_{L1}, S'_{L1}, N'_{R1}, S'_{R1}$	contact center between the ball and raceway after deformation when $F_a < 2.83\ F_p$
$N'_{L2}, S'_{L2}, N'_{R2}, S'_{R2}$	contact center between the ball and raceway after deformation when $F_a > 2.83\ F_p$
O_B, O_N, O_S	curvature center of ball/nut raceway/screw raceway under initial contact state
O'_B, O'_N	curvature center of ball/nut raceway after contact deformation
P_s	screw pitch
r	ball radius
r_n, r_s	nut/screw track curvature radius
$v_b^{xn}, v_b^{yn}, v_n^{xn}, v_n^{yn}$	ball/screw sliding velocity
R	screw pitch radius
R_{b-si}, R_{b-ni}	sliding-rolling ratios between ball and screw/nut
R_k	effective curvature radius of the raceway
$S_{bs}\ (t_i)$	creep length value in rolling motion
t_b	raceway curvature ratio
v	feed rate
$v_b^{xs}, v_b^{ys}, v_s^{xs}, v_s^{ys}$	ball/screw sliding velocity in x_s/y_s direction
$v_{b-n}^{xn}, v_{b-n}^{yn}$	average rolling velocity in x_n/y_n direction
$v_{b-s}^{xs}, v_{b-s}^{ys}$	average rolling velocity in x_s/y_s direction
v_{bs-ssi}, v_{bn-sni}	ball velocity relative to the screw/nut
$v_{b-si}^{uc}, v_{b-ni}^{uc}$	ball center velocity relative to screw/nut
$v_{rbs}^{xn}, v_{rbs}^{yn}$	sliding velocity in x_n/y_n direction
$v_{rbs}^{xs}, v_{rbs}^{ys}$	sliding velocity in x_s/y_s direction
V_{b-s}, V_{b-n}	wear amounts of one cycle
V_{b-n}^{L}, V_{b-n}^{R}	wear amount between ball and left/right nut in one cycle
V_{b-s}^{L}, V_{b-s}^{R}	wear amount of ball in left/right nut with screw in one cycle
$V_{b-s}^{L1}(t), V_{b-n}^{L1}(t), V_{b-s}^{R1}(t), V_{b-n}^{R1}(t)$	wear amount of No. 1 ball in left/right nut with the screw/nut in one cycle
$x_b^{xn}, x_b^{yn}, x_n^{xn}, x_n^{yn}$	ball/screw contact position in x_n/y_n direction
$x_b^{xs}, x_b^{ys}, x_s^{xs}, x_s^{ys}$	ball/screw contact position in x_s/y_s
$\theta_{ni}^{L1}, \theta_{si}^{L1}$	contact angle between No. i ball and left nut/screw under Fa<2.83Fp
$\theta_{ni}^{R1}, \theta_{si}^{R1}$	contact angle between No. i ball and right nut/screw under Fa<2.83Fp
$\theta_{ni}^{L2}, \theta_{si}^{L2}$	contact angle between No. i ball and left nut/screw under Fa>2.83Fp
$\theta_{ni}^{R2}, \theta_{si}^{R2}$	contact angle between No. i ball and right nut/screw under Fa>2.83Fp
ϑ	the angle between the 2-axis and the b-axis (Ref. [2])
α	helix angle
$\delta_a^{L1}, \delta_a^{R1}$	axial deformation between left/right nut and screw under Fa<2.83Fp
$\delta_a^{L2}, \delta_a^{R2}$	axial deformation between left/right nut and screw under Fa>2.83Fp
ε	ratio of axial load to preload
ϕ_i^u	phase angle of No. i ball
φ	center angle between two adjacent balls
γ	phase angle of No. 1 ball
η	transmission efficiency without preload
λ	equivalent friction angle
θ_{L1}, θ_{R1}	contact angle between ball in left/right nut and raceway under Fa<2.83Fp
θ_{L2}, θ_{R2}	contact angle between ball in left/right nut and raceway under Fa>2.83Fp
$\theta'_{L1}, \theta'_{R1}, \theta'_{L2}, \theta'_{R2}$	change value of initial contact angle $\theta_{L1}/\theta_{R1}/\theta_{L2}/\theta_{R2}$
ω	rotating speed of screw
$\omega_b, \omega_n, \omega_t$	projection of ω_{br} in $B/N/T$ direction

ω_{br}	ball spin angular velocity
ω_{ni-b}	angular velocity of nut relative to ball
ω_N	nut angular velocity
ω_{si-b}	angular velocity of screw relative to ball
ζ_{xn}, ζ_{yn}	creep rate in x_n/y_n direction
ζ_{xs}, ζ_{ys}	creep rate in x_s/y_s direction
ψ	the angle between the U-axis and the 2-axis (Ref. [2])
Δp	precision loss values due to sliding-rolling mixed motion

I. INTRODUCTION

Ball screws are often used as precision transmission components in the aerospace, CNC machine tool, and electromechanical equipment industries. Precision loss of the ball screw will directly affect the performance of precision equipment. Precision retention is defined as the ability to maintain a certain level precision under specific operating conditions over a certain period of time. Mixed sliding-rolling motion can have considerable influence on ball screw precision loss. Moreover, reducing the rate of precision loss can improve precision retention.

To date, studies on the precision loss of ball screws due to sliding and rolling motion have typically focused on kinematic and static analyses [1]–[6] or creep theory [7], [8]. By combining sliding motion analysis with Archard theory [9], a ball screw precision loss model for analyzing sliding motion behavior was previously established [10]–[13]. Wei *et al.* [10] investigated wear rates of ball screws under various operating conditions and described the relationship between preload and wear rate. Zhou *et al.* [11] introduced an accuracy loss model and examined the influence of sliding speed and sliding motion on precision loss of the screw raceway. Liu *et al.* [12] improved the precision loss model by considering the real contact area between the ball and the raceway, thereby improving the accuracy of the precision loss calculation. Further studies were also performed by Wei *et al.* [10], Zhou *et al.* [11], and Liu *et al.* [12] under constant working conditions, i.e., constant axial load and constant feed rate. In contrast, Cheng *et al.* [13] studied the ball screw precision loss characteristics caused by sliding motion under time-varying axial loads and feed rates. In addition, rolling motion analysis was combined with creep theory [7], [8]. Xu *et al.* [8] established a friction force model of the ball screw.

Previously derived precision loss characteristics have laid the foundation for the optimized design of the ball screw for precision retention. Thus far, studies on the optimization of structural parameters of the ball screw have been limited to the transmission efficiency [3], [4], stiffness [1], [14], servo structure [15], [16], preload [17] and active suspension [18]. Based on data from experimental studies of the ball screw actuator, Zhao *et al.* [18] proposed an active suspension system with a novel double vibration reduction structure. Riaz *et al.* [19] used the optimized softmax function to identify defects in ball screw actuators, including mechanical friction, backlash, and fatigue failure. However, fewer studies have optimized structural parameters of the ball screw for precision retention. Miura *et al.* [20] adopted the small-ball concept to optimize the ball screw position accuracy by reducing fluctuations in the contact load.

Previous research has effectively optimized the ball screw based on transmission efficiency, stiffness, servo structure, preload, and structural parameters. To the authors' knowledge, the ball screw has not been optimized for precision retention while considering the effects of mixed sliding-rolling motion. Thus, precision loss of the ball screw under mixed sliding-rolling motion behavior merits further attention. In this study, operating conditions and structural parameters affecting the precision loss of the ball screw were analyzed. Then, based on precision loss, the structural parameters were optimized to improve precision retention.

The rest of paper is organized as follows: In Section 2, a method based on kinematic theory for calculating the precision loss of the ball screw caused by mixed sliding-rolling motion is introduced. In Section 3, the calculated precision loss is used to analyze the operating conditions and structural parameters associated with precision loss. Section 4 presents an optimization analysis for precision retention based on the precision loss characteristics under mixed sliding-rolling motion. In Section 5, the objective function and optimization constraints are presented, and are used to optimize structural parameters of the ball screw with the overall aim of improving precision retention. The main conclusions of the study are summarized in Section 6.

II. PRECISION DEGRADATION UNDER MIXED SLIDING-ROLLING MOTION

During operation of the ball screw, rolling and sliding movement between the ball and the raceway occur. Precision loss of the ball screw due to wear can be calculated separately for sliding and rolling motion using the Archard model [9] and creep theory [8], respectively.

A. PRECISION DEGRADATION DUE TO SLIDING MOTION

The contact area between the ball and raceway is an ellipse, however, the actual contact area is only a small region of the ellipse, as shown in Fig. 1. Precision degradation due to sliding wear between ball and screw/nut raceway can be expressed as

$$h_{sbs} = \frac{C_{b-s}V_{b-s}}{A_s L_{b-s}} A_{rs} \tag{1a}$$

$$h_{sbn} = \frac{C_{b-n}V_{b-n}}{A_n L_{b-n}} A_{rn} \tag{1b}$$

where C_{b-s}, C_{b-n} are the cycle number and V_{b-s}, V_{b-n} are wear during one cycle of the ball relative to the screw/nut raceway, respectively; A_s, A_n are the nominal contact area between ball and screw/nut, respectively; A_{rs}, A_{rn} are the actual contact area between ball and screw/nut, respectively;

L_{b-s} and L_{b-n} are the length of the screw/nut raceway as well as the abraded areas, Then,

$$L_{b-k} = L_k / \sin\alpha \tag{2}$$

$$A_k = \pi a_k b_k = \pi \left(\frac{6N_H R_k F_k}{\pi E^*}\right)^{2/3} \tag{3a}$$

$$A_{rk} = \left[\frac{\left(\frac{4}{\pi E^*}\frac{r_k r}{r_k - r}\right)}{\pi\left(r_k - r\right)}\right]^{\left(\frac{1}{r}-\frac{1}{r_k}\right)} \frac{D_f}{2 - D_f} a_{Lk} \tag{3b}$$

$$\begin{aligned} V_{b-s} &= V_{b-s}^L + V_{b-s}^R \\ &= \left[V_{b-s}^{L1}(t) + \cdots + V_{b-s}^{LM}(t)\right] \\ &\quad + \left[V_{b-s}^{R1}(t) + \cdots + V_{b-s}^{RM}(t)\right] \end{aligned} \tag{4a}$$

$$\begin{aligned} V_{b-n} &= V_{b-n}^L + V_{b-n}^R \\ &= \left[V_{b-n}^{L1}(t) + \cdots + V_{b-n}^{LM}(t)\right] \\ &\quad + \left[V_{b-n}^{R1}(t) + \cdots + V_{b-n}^{RM}(t)\right] \end{aligned} \tag{4b}$$

When $k = s$, Eq. (2) represents L_{b-s}; when $k = n$, Eq. (2) represents L_{b-s}. In Eq. (3a), when $k = s$, a_k, b_k are the long/short axes of the contact ellipse between ball and nut, respectively; when $k = n$, a_n, b_n are the long/short axis of the contact ellipse between ball and nut; N_H is the Hertz contact area parameter; R_k is the effective curvature radius of the raceway; F_k is the contact load between the ball and raceway. E^* is the equivalent elastic modulus of the material. When $k = s$, Eq. (3a) represents A_s; when $k = n$, Eq. (3a) represents A_n. In Eq. (3b), r_k represents the raceway curvature radius, fractal parameter $D_f = 1.62$, and a_{Lk} is the maximum contact area [12]. When $k = s$, Eq. (3) represents A_{rs}; when $k = n$, Eq. (3) represents A_{rn}; V_{b-s}^L, V_{b-s}^R is the amount of wear of the ball in left/right nut with screw in one cycle; V_{b-n}^L, V_{b-n}^R represents the amount of wear between ball and left/right nut during one cycle, respectively.

The contact state of the ball screw varies with the axial load and preload. The preload tends to decay during operation, however, preload attenuation is a lengthy process, moreover, the preload cannot be directly measured. Zhou *et al.* [6] described the relationship between the preload and no-load drag torque to indirectly obtain the preload. Based on this method, a preload attenuation law was introduced and used to predict preload attenuation [21].

In this study, the feed rate of screw was 240 mm/min and 0.96 million revolutions were performed in 800 h. The support vector machine (SVM) was used to predict the preload attenuation rate of ball screw [21]. The results show that from 0–0.96 million revolutions, the preload attenuation rate changes from 0 to approximately 16.91%. After 800 h, the attenuated preload value is about 224.90 N. That is, the average preload attenuation rate is about 0.2811 N/h. Fig. 1 shows the contact state between the ball and the raceway under different working conditions.

In Fig. 1, the actual contact angle includes the initial contact angle and the change in contact angle due to contact deformation.

From the force balance analysis of Fig. 1(a),

$$\begin{cases} F_p^{L2}(t) + F_a^{L2} = \sum_{i=1}^{M_{bL}} F_{si}^{L2} \sin\theta_{si}^{L2} \cos\alpha \\ F_a^{R2} - F_p^{R2}(t) = \sum_{i=1}^{M_{bR}} F_{si}^{R2} \sin\theta_{si}^{R2} \cos\alpha \\ F_a^{L2} + F_a^{R2} = F_a \\ \left(F_p^{L2}(t) + F_a^{L2}\right)^{\frac{2}{3}} - \left(F_p^{L2}(t)\right)^{\frac{2}{3}} \\ \qquad = \left(F_p^{R2}(t)\right)^{\frac{2}{3}} + \left(F_a^{R2} - F_p^{R2}(t)\right)^{\frac{2}{3}} \end{cases} \tag{5}$$

Similarly, the force balance analysis of Fig. 1(b) gives

$$\begin{cases} F_p^{L1}(t) + F_a^{L1} = \sum_{i=1}^{M_{bL}} F_{si}^{L1} \sin\theta_{si}^{L1} \cos\alpha \\ F_p^{R1}(t) - F_a^{R1} = \sum_{i=1}^{M_{bR}} F_{si}^{R1} \sin\theta_{si}^{R1} \cos\alpha \\ F_a^{L1} + F_a^{R1} = F_a \\ \left(F_p^{L1}(t) + F_a^{L1}\right)^{\frac{2}{3}} + \left(F_p^{R1}(t) - F_a^{R1}\right)^{\frac{2}{3}} = 2\left(F_p^{L1}(t)\right)^{\frac{2}{3}} \end{cases} \tag{6}$$

The contact angle changes according to the amount of contact deformation, which affects the distribution of the contact load. Fig. 2 presents a schematic diagram of contact deformation under the axial load and preload.

Parameters in Fig. 2 are defined in the Nomenclature. The amount of contact deformation, δ_a^{L1}, δ_a^{R1}, δ_a^{L2}, and δ_a^{R2}, can be calculated using Hertz contact theory. Assuming the preload and axial load cause contact deformation, the initial contact angles change from θ_{L1}, θ_{R1}, θ_{L2}, and θ_{R2} to θ_{ni}^{L1}, θ_{ni}^{R1}, θ_{ni}^{L2}, and θ_{ni}^{R2}, respectively. representing an increase in θ'_{L1}, θ'_{R1}, θ'_{L2}, and θ'_{R2}, respectively.

$$\begin{cases} \theta_{ni}^{L1} = \arcsin \dfrac{L_{SN}\sin\theta_{L1} + \frac{\delta_a^{L1}}{\cos\alpha}}{\sqrt{\left(L_{SN}\cos\theta_{L1}\right)^2 + \left[L_{SN}\sin\theta_{L1} + \frac{\delta_a^{L1}}{\cos\alpha}\right]^2}} \\ \theta'_{L1} = \theta_{ni}^{L1} - \theta_{L1} \end{cases} \tag{7a}$$

$$\begin{cases} \theta_{ni}^{R1} = \arcsin \dfrac{L_{SN}\sin\theta_{R1} + \frac{\delta_a^{R1}}{\cos\alpha}}{\sqrt{\left(L_{SN}\cos\theta_{R1}\right)^2 + \left[L_{SN}\sin\theta_{R1} + \frac{\delta_a^{R1}}{\cos\alpha}\right]^2}} \\ \theta'_{R1} = \theta_{ni}^{R1} - \theta_{R1} \end{cases} \tag{7b}$$

$$\begin{cases} \theta_{ni}^{L2} = \arcsin \dfrac{L_{SN}\sin\theta_{L2} + \frac{\delta_a^{L2}}{\cos\alpha}}{\sqrt{\left(L_{SN}\cos\theta_{L2}\right)^2 + \left[L_{SN}\sin\theta_{L2} + \frac{\delta_a^{L2}}{\cos\alpha}\right]^2}} \\ \theta'_{L2} = \theta_{ni}^{L2} - \theta_{L2} \end{cases} \tag{7c}$$

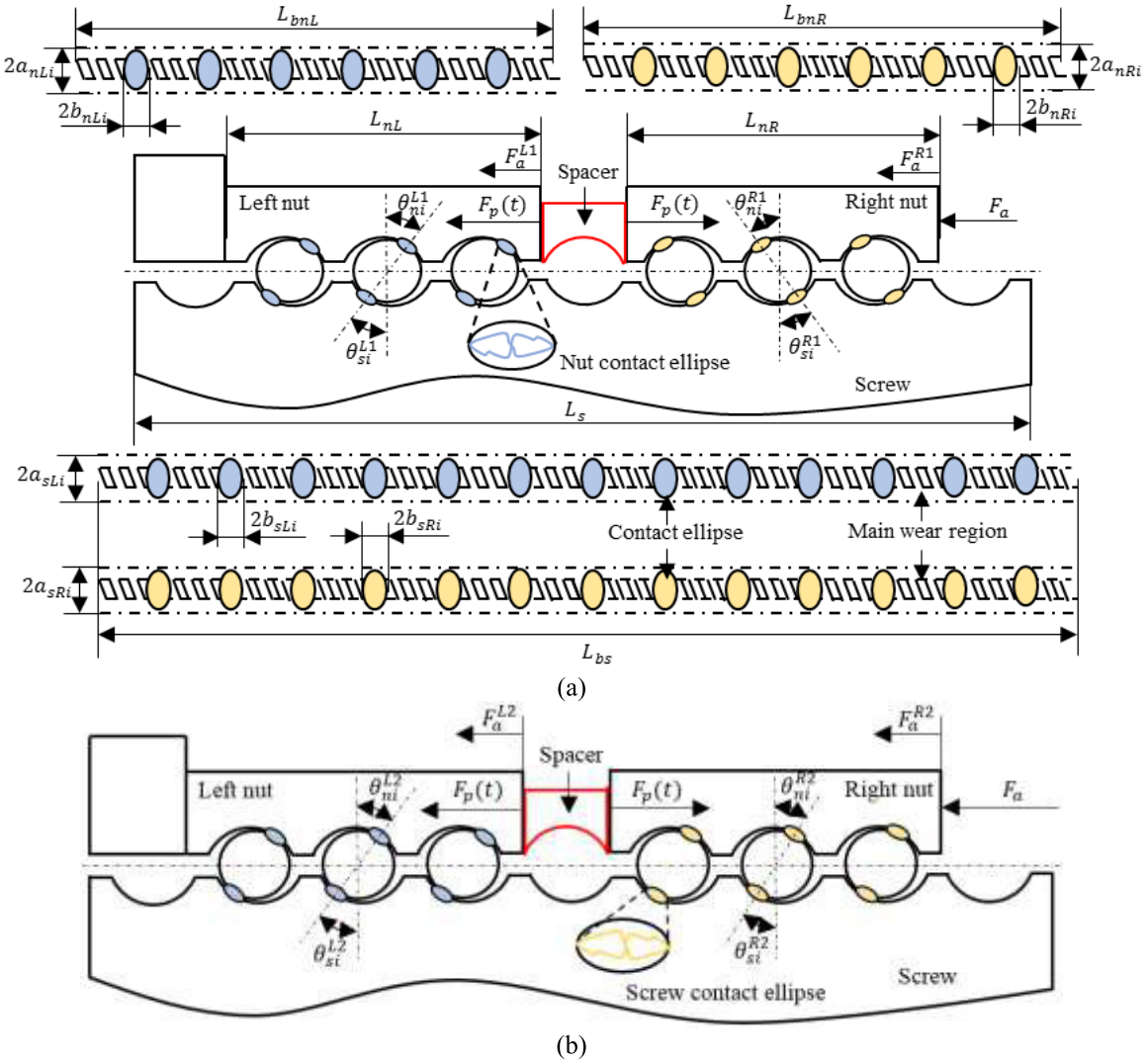

FIGURE 1. Contact state and wear of ball screw under different working conditions: (a) Axial force is 2.83 times less than the preload; (b) Axial force is 2.83 times greater than the preload.

$$\begin{cases} \theta_{ni}^{R2} = \arcsin \dfrac{L_{SN} \sin\theta_{R2} + \frac{\delta_a^{R2}}{\cos\alpha}}{\sqrt{(L_{SN}\cos\theta_{R2})^2 + \left[L_{SN}\sin\theta_{R2} + \frac{\delta_a^{R2}}{\cos\alpha}\right]^2}} \\ \theta'_{R2} = \theta_{ni}^{R2} - \theta_{R2} \end{cases} \tag{7d}$$

where L_{SN} is the distance between the curvature center of the screw and nut raceway in the initial contact state, expressed as

$$L_{SN} = |O_N O_S| = |r_N + r_S - D_b| \tag{8}$$

where r_N, r_S are the nut/screw track curvature radius and D_b is the ball diameter.

From t_{ssi} to t_{ssi+1}, the amount of wear of the ball and screw/nut can be expressed as

$$V_{b-si}^{u}(t_{ssi}) = \int_{t_{ssi}}^{t_{ssi+1}} v_{b-si}^{uc}(t_{ssi})dt = \int_{t_{ssi}}^{t_{ssi+1}} k_{bs}\frac{F_{si}^{uc}}{H_{b-s}}L_{bsi}dt \tag{9a}$$

$$V_{b-ni}^{u}(t_{nsi}) = \int_{t_{nsi}}^{t_{nsi+1}} v_{b-ni}^{uc}(t_{nsi})\,dt = \int_{t_{nsi}}^{t_{nsi+1}} k_{bn}\frac{F_{ni}^{uc}}{H_{b-n}}L_{bni}dt \tag{9b}$$

where v_{b-si}^{uc} and v_{b-ni}^{uc} are the velocity of the ball center relative to the screw and nut, respectively, in the spiral direction. When $u = L$, v_{b-si}^{uc} is the velocity of the ball in the left nut relative to the screw, v_{b-ni}^{uc} is the velocity of the ball relative to the left nut; When $u = R$, v_{b-si}^{uc} is the velocity of the ball in the right nut relative to the screw and v_{b-ni}^{uc} is the velocity of the ball relative to the right nut, expressed as [2], [22]

$$\begin{aligned} v_{b-si}^{uc} &= \omega_n r\sin\theta_{ni}^{uc} - \omega_b r\cos\theta_{ni}^{uc} \\ &\quad - \omega\left(\frac{R}{\cos\alpha} + r\cos\theta_{ni}^{uc}\cos\alpha\right) \end{aligned} \tag{10a}$$

$$\begin{aligned} v_{n-bi}^{uc} &= v_{b-s} - \omega_n r\sin\theta_{ni}^{uc} + \omega_b r\cos\theta_{ni}^{uc} \\ &\quad + \omega\left(\frac{R}{\cos\alpha} + r\cos\alpha\cos\theta_{ni}^{uc}\right) \end{aligned} \tag{10b}$$

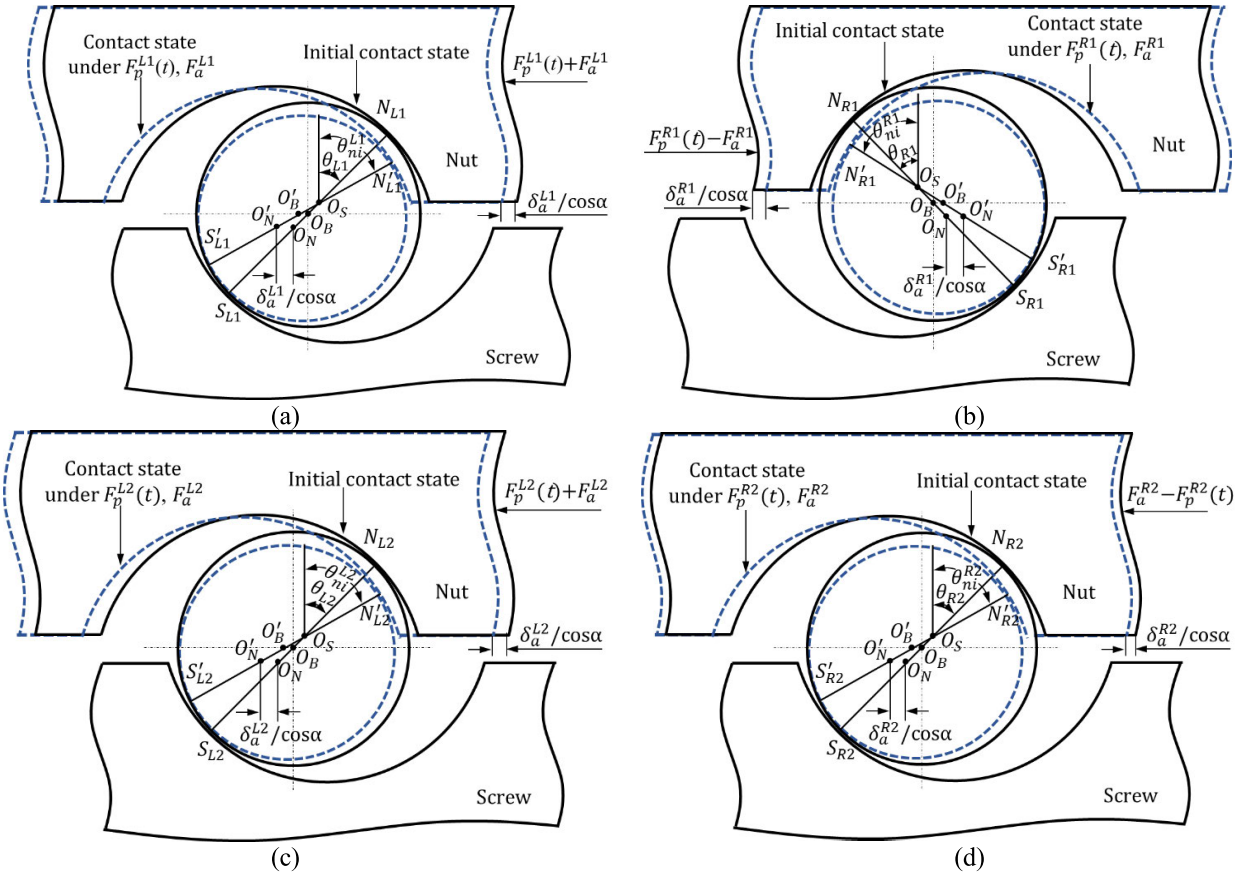

FIGURE 2. Deformation and contact state between ball and raceway under axial force and preload: (a) Deformation between the left nut and screw when the axial force 2.83 times less than the preload force; (b) Deformation between the right nut and screw when the axial force is 2.83 times less than the preload force; (c) Deformation between the left nut and screw when the axial force 2.83 times greater than the preload force; (d) Deformation between the right nut and screw when the axial force is 2.83 times greater than the preload force.

In Eq. (9a–b) and Eq. (10a–b), when $F_a < 2.83F_p$, $c = 1$; when $F_a > 2.83F_p$, $c = 2$.

Sliding distances of the screw/nut relative to the i-th ball, L_{bsi} and L_{bni}, respectively, are

$$L_{bsi} = \frac{R_{b-si}\omega_{si-b} r\cos\alpha}{\pi\left(1+R_{b-si}\right)v_{bs-ssi}R}\sqrt{R^2+\left(\frac{L}{2\pi}\right)^2} \times\sqrt{\left(R-r\cos\theta_{si}^{uc}\right)^2+\left(\frac{P_s}{2\pi}\right)^2} \tag{11a}$$

$$L_{bni} = \frac{R_{b-ni}\omega_{ni-b} r\cos\alpha}{\pi\left(1+R_{b-ni}\right)v_{bn-sni}R}\sqrt{R^2+\left(\frac{L}{2\pi}\right)^2} \times\sqrt{\left(R-r\cos\theta_{ni}^{uc}\right)^2+\left(\frac{P_s}{2\pi}\right)^2} \tag{11b}$$

where v_{bs-ssi} and v_{bn-sni} are the velocity of the ball relative to the screw/nut at the contact point; R_{b-si} and R_{b-ni} are the sliding-rolling ratios between the ball and screw/nut, respectively [2], [13]; ω_{si-b} is the angular velocity of the screw relative to the ball and ω_{ni-b} is the angular velocity of the nut relative to the ball, expressed as (12a) and (12b) shown at the bottom of the next page.

B. PRECISION LOSS DUE TO ROLLING MOTION

According to Kalker's empirical theory [23], partial sliding and partial sticking phenomena may occur in the rolling contact area. A schematic diagram of rolling contact between the ball and raceway is presented in Fig. 3 (see Nomenclature for parameter definitions).

At time t_i, rolling wear of the ball and the screw raceway can be written as

$$h_{rbs} = h_{rbs}\left(t_{i-1}\right) + k_{bs}f_{ixs}\left\|S_{bs}\left(t_i\right) - S_{bs}\left(t_{i-1}\right)\right\| \tag{13}$$

where $h_{rbs}\left(t_{i-1}\right)$ is the wear depth of a ball and screw raceway at time t_{i-1} and f_{ixs} can be written as

$$f_{ixs} \approx \frac{F_{si}^{uc}}{4c_{xs}a_{ys}} \tag{14}$$

According to Eq. (13), the cumulative wear depth of the rolling contact area between the ball and the screw in the direction x_s/y_s can be obtained as

$$h_{rbs}^{xs} = h_{rbs}^{xs}\left(t_A^{xs}\right) + \int_{t_A^{xs}}^{t_i^{xs}} k_{bs}f_{ixs}v_{rbs}^{xs}dt_i^{xs}, \quad t_i^{xs} < t_C^{xs} \tag{15a}$$

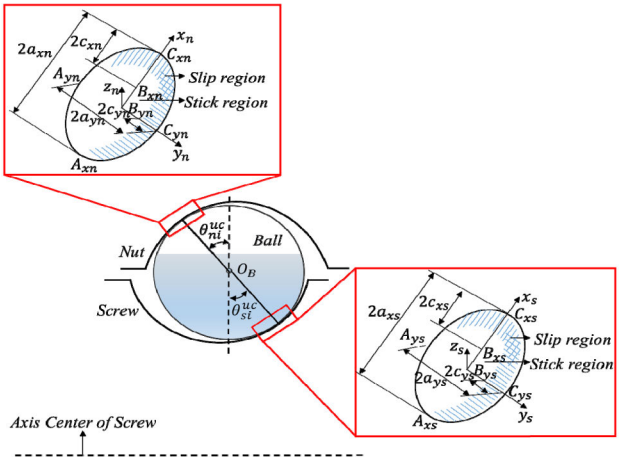

FIGURE 3. Rolling contact between ball and raceway.

$$\begin{cases} h_{rbs}^{ys} = h_{rbs}^{ys}\left(t_A^{ys}\right) + \int_{t_A^{ys}}^{t_i^{ys}} k_{bs} f_{iys} v_{rbs}^{ys} dt_i^{ys}, \; t_i^{ys} < t_C^{ys} \\ f_{iys} \approx \dfrac{F_{si}^{uc}}{4 c_{ys} a_{xs}} \end{cases} \tag{15b}$$

where $v_{rbs}^{xs}/v_{rbs}^{ys}$ is the sliding velocity in the x_s/y_s direction (see Nomenclature for parameter definitions).

$$\begin{cases} v_{rbs}^{xs} = v_{b-s}^{xs}\zeta_{xs} + v_b^{xs}\partial\left(d_b^{xs} - d_s^{xs}\right)/\partial x_b^{xs} \\ \qquad + v_s^{xs}\partial\left(d_b^{xs} - d_s^{xs}\right)/\partial x_s^{xs} \\ \left|v_b^{xs}\right| = \left|v_s^{xs}\right| = \left|\left(r\omega\cos\theta_{si}^{uc} - R\omega\right)\sin\phi_i^u\right. \\ \qquad \left. + r\omega\sin\alpha\sin\theta_{si}^{uc}\cos\phi_i^u\right| \\ \phi_i^u = \gamma + \varphi\,(i-1) \end{cases} \tag{16a}$$

$$\begin{cases} v_{rbs}^{ys} = v_{b-s}^{ys}\zeta_{ys} + v_b^{ys}\partial\left(d_b^{ys} - d_s^{ys}\right)/\partial x_b^{ys} \\ \qquad + v_s^{ys}\partial\left(d_b^{ys} - d_s^{ys}\right)/\partial x_s^{ys} \\ \left|v_b^{ys}\right| = \left|v_s^{ys}\right| = \left|\left(R\omega - r\omega\cos\theta_{si}^{uc}\right)\cos\phi_i^u\right. \\ \qquad \left. + r\omega\sin\alpha\sin\theta_{si}^{uc}\sin\phi_i^u\right| \end{cases} \tag{16b}$$

Then, the average rolling velocity in the x_s/y_s direction $v_{b-s}^{xs}/v_{b-s}^{ys}$ is (17a), (17b) as shown at the bottom of the next page.

ζ_{xs}/ζ_{ys} is the creep rate in the x_s/y_s direction [8], calculated as (18a), (18b) as shown at the bottom of the next page.

Similarly, the cumulative wear depth of the rolling contact area between the ball and the nut in the x_n/y_n direction can be written as

$$h_{rbn}^{xn} = h_{rbn}^{xn}\left(t_A^{xn}\right) + \int_{t_A^{xn}}^{t_i^{xn}} k_{bn} f_{ixn} v_{rbn}^{xn} dt_i^{xn}, \quad t_i^{xn} < t_C^{xn} \tag{19a}$$

$$h_{rbn}^{yn} = h_{rbn}^{yn}\left(t_A^{yn}\right) + \int_{t_A^{yn}}^{t_i^{yn}} k_{bn} f_{iyn} v_{rbn}^{yn} dt_i^{yn}, \quad t_i^{yn} < t_C^{yn} \tag{19b}$$

According to Eq. (14) and Fig. 3, f_{ixn} and f_{iyn} can be derived by analogy. From Eq. (18a-b), ψ and ϑ can be acquired [2], then ω_N can be obtained as

$$\omega_N = -\omega\left(\frac{R}{\cos\alpha} + r\cos\theta_{si}^{uc}\cos\alpha\right) \tag{20}$$

III. PRECISION LOSS MODEL AND INFLUENCING FACTORS

A. PRECISION LOSS MODEL

Precision loss is the difference between the positioning error at the end of the operation and the initial positioning error in the stable wear stage. According to the model of precision loss due to sliding wear (Section 2.1) and combining Eqs. (9a), (10a) and (11a), V_{b-s} can be obtained as

$$\begin{aligned} V_{b-s} &= M\left[V_{b-s}^{Lc}(t)\frac{b_s^{Lc}}{i_t} + V_{b-s}^{Rc}(t)\frac{b_s^{Rc}}{i_t}\right] \\ &= M\left(k_{bs}\frac{F_{si}^{Lc}L_{bsi}}{H_{b-s}}\frac{b_s^{Lc}}{i_t} + k_{bs}\frac{F_{si}^{Rc}L_{bsi}}{H_{b-s}}\frac{b_s^{Rc}}{i_t}\right) \end{aligned} \tag{21}$$

where i_t is the number of leads (see Table 1). Combining Eqs. (1a) and (21), the precision loss due to sliding wear in the stroke direction can be written as

$$\begin{aligned} H_{sbs} = \frac{\cos\alpha}{\sin\theta_{si}^{uc}}\int_0^{L_{b-s}} &\frac{C_{b-s}Mk_{bs}L_{bsi}}{H_{b-s}i_t} \\ &\times\left(\frac{F_{si}^{Lc}b_s^{Lc}}{A_s^{Lc}}A_{rs}^{Lc} + \frac{F_{si}^{Rc}b_s^{Rc}}{A_s^{Rc}}A_{rs}^{Rc}\right)dl \end{aligned} \tag{22}$$

Similarly, combining Eqs. (9b), (10b), and (11b), V_{b-n} can be obtained. Based on Eq. (1b), precision loss due to sliding wear, H_{sbn}, can be expressed as

$$\begin{aligned} H_{sbn} = \frac{\cos\alpha}{\sin\theta_{ni}^{uc}}\int_0^{L_{b-n}} &\frac{C_{b-n}Mk_{bn}L_{bni}}{H_{b-n}i_t} \\ &\times\left(\frac{F_{ni}^{Lc}b_n^{Lc}}{A_n^{Lc}}A_{rn}^{Lc} + \frac{F_{ni}^{Rc}b_n^{Rc}}{A_n^{Rc}}A_{rn}^{Rc}\right)dl \end{aligned} \tag{23}$$

Based on Section 2.2.1 and Eq. (16a), the relationship between the number of rolling cycles and the rolling wear depth in the x_s-direction can be written as where $n_{xs} = MC_{b-s}$. According to Eq. (3), $c_{xs}a_{ys}$ can be calculated as [14], [25], [26],

$$c_{xs}a_{ys} \approx \frac{1}{8}\left(\frac{6N_H r_s F_{si}^{uc}}{\pi E_s}\right)^{2/3} \tag{25}$$

$$\omega_{si-b} = \frac{r_s\left(r + r_n\cos\theta_{ni}^{uc}\right)\cos\alpha\cos\left(\alpha - \theta_{si}^{uc}\right)\omega}{r_n\left(r - r_s\cos\theta_{si}^{uc}\right)\cos\left(\alpha - \theta_{ni}^{uc}\right) + r_s\left(r + r_n\cos\theta_{ni}^{uc}\right)\cos\left(\alpha - \theta_{si}^{uc}\right)} \tag{12a}$$

$$\omega_{ni-b} = \frac{-r_n\left(r - r_s\cos\theta_{si}^{uc}\right)\cos\left(\alpha - \theta_{ni}^{uc}\right)\omega}{r_n\left(r - r_s\cos\theta_{si}^{uc}\right)\cos\left(\alpha - \theta_{ni}^{uc}\right) + r_s\left(r + r_n\cos\theta_{ni}^{uc}\right)\cos\left(\alpha - \theta_{si}^{uc}\right)} \tag{12b}$$

Similarly, rolling wear depth in the y_s direction can be written as

$$h_{rbs}^{ys}(n) = \frac{n_{ys} k_{bs} F_{si}^{uc} a_{ys} \zeta_{ys} \left(\delta_a^{uc} - r\right) r\omega_t}{4 c_{ys} a_{xs}} \tag{26}$$

where $n_{ys} = n_{xs} = MC_{b-s}$ and $c_{ys}a_{xs}$ can be calculated as

$$c_{ys}a_{xs} \approx \frac{1}{9}\left(\frac{6N_H r_s F_{si}^{uc}}{\pi E_s}\right)^{2/3} \tag{27}$$

Rolling wear depth in the x_n/y_n direction can be written (28) as shown at the bottom of the next page.

Rolling wear depth in the y_n direction can be written as

$$h_{rbn}^{yn}(n) = \frac{n_{yn} k_{bn} F_{ni}^{uc} a_{yn} \zeta_{yn} \left(r - \delta_a^{uc}\right) r\omega_t}{4 c_{yn} a_{xn}} \tag{29}$$

According to Eqs. (24), as shown at the bottom of this page, and (25), the precision loss due to rolling wear depth in the x_s direction is

$$H_{rbs}^{xs} = \frac{\cos\alpha}{\sin\theta_{si}^{uc}} \int_0^{L_{b-s}} h_{rbs}^{xs}(n)\, dl \tag{30}$$

Similarly, based on Eqs. (27) and (28), the precision loss due to rolling wear depth in the y_s direction is

$$H_{rbs}^{ys} = \frac{\cos\alpha}{\sin\theta_{si}^{uc}} \int_0^{L_{b-s}} h_{rbs}^{ys}(n)\, dl \tag{31}$$

The precision loss due to rolling wear depth in the x_n and y_n directions can be defined, separately, as

$$H_{rbn}^{xn} = \frac{\cos\alpha}{\sin\theta_{ni}^{uc}} \int_0^{L_{b-n}} h_{rbn}^{xn}(n)\, dl \tag{32a}$$

$$H_{rbn}^{yn} = \frac{\cos\alpha}{\sin\theta_{ni}^{uc}} \int_0^{L_{b-n}} h_{rbn}^{yn}(n)\, dl \tag{32b}$$

Combining Eqs. (22), (23), and (30)–(32b), the precision loss considering mixed sliding-rolling motion can be obtained as

$$\Delta p = H_{sbs} + H_{sbn} + H_{rbs}^{xs} + H_{rbs}^{ys} + H_{rbn}^{xn} + H_{rbn}^{yn} \tag{33}$$

TABLE 1. Initial parameters of ball screw.

Parameters	Value	Unit
Nominal diameter of ball screw	50	mm
Ball diameter	6.75	mm
Nut track curvature radius	3.673	mm
Screw track curvature radius	3.673	mm
Contact angle	45	degree
Helix angle	4.35	degree
Lead	12	mm
Axial length of nuts	80	mm
Number of balls	136	/
Rows × Turns × Leads	2×2.5×1	/
Raceway curvature ratio	1.09	/
Screw hardness	62	HRC
Nut hardness	62	HRC
Young's modulus	205	GPa
Poisson's ratio	0.3	/
Lubrication mode	Grease	/
Boundary wear coefficient	3.2E-11	/

B. PRECISION LOSS ANALYSIS AND EXPERIMENT

For the experiment, the preload was set to 1330 N and the axial load was 2500 N. The feed rate of screw was 240 mm/min. Lubricating grease (KOC301) was used and all tests were carried out at ambient temperature (23°C). The operating time under each condition was 500 h. Parameters of the ball screw (W5017-C2Z12) are listed in Table 1.

Fig. 4 presents a flowchart of the process for calculating the ball screw mechanism (BSM) precision loss due to mixed sliding-rolling motion.

In this study, V_μ (with a tested travel range of 400 mm) was selected as the precision loss index. The precision loss value was then calculated as the difference between the initial value V_μ^0 and V_μ^t were recorded at various time points. The cumulative wear depth in the stroke direction corresponds to the BSM precision loss [4], [11], [12]. Precision degradation of the BSM due to accumulated wear caused by sliding motion of the ball and screw/nut can be obtained using Eqs. (22) and (23), respectively. Fig. 5 compares the BSM precision loss due to sliding motion wear obtained using the model presented in this article and values obtained

$$v_{b-s}^{xs} = \frac{r\left(\delta_a^{uc} - r\right)\left(\omega_n \cos\theta_{si}^{uc} + \omega_b \sin\theta_{si}^{uc}\right) + \omega r R_{bs}\left[\left(r - \delta_a^{uc}\right)\cos\theta_{si}^{uc} - R\right]}{2} \tag{17a}$$

$$v_{b-s}^{ys} = \frac{r\left(\delta_a^{uc} - r\right)\omega_t}{2} \tag{17b}$$

$$\zeta_{xs} = \frac{2\left(\delta_a^{uc} - r\right)\left(\omega\cos\theta_{si}^{uc} - \omega_{br}\sin\psi\cos\theta_{si}^{uc} - \omega_{br}\cos\psi\cos\vartheta\sin\theta_{si}^{uc}\right) + \omega R}{\omega R + \left(r - \delta_a^{uc}\right)\left(\omega_n\cos\theta_{si}^{uc} + \omega_b\sin\theta_{si}^{uc} - \omega\cos\theta_{si}^{uc}\right)} \tag{18a}$$

$$\zeta_{ys} = \frac{2\left(\delta_a^{uc} - r\right)\omega_{br}\cos\psi\sin\vartheta}{\omega R + \left(r - \delta_a^{uc}\right)\left(\omega_n\cos\theta_{si}^{uc} + \omega_b\sin\theta_{si}^{uc} - \omega\cos\theta_{si}^{uc}\right)} \tag{18b}$$

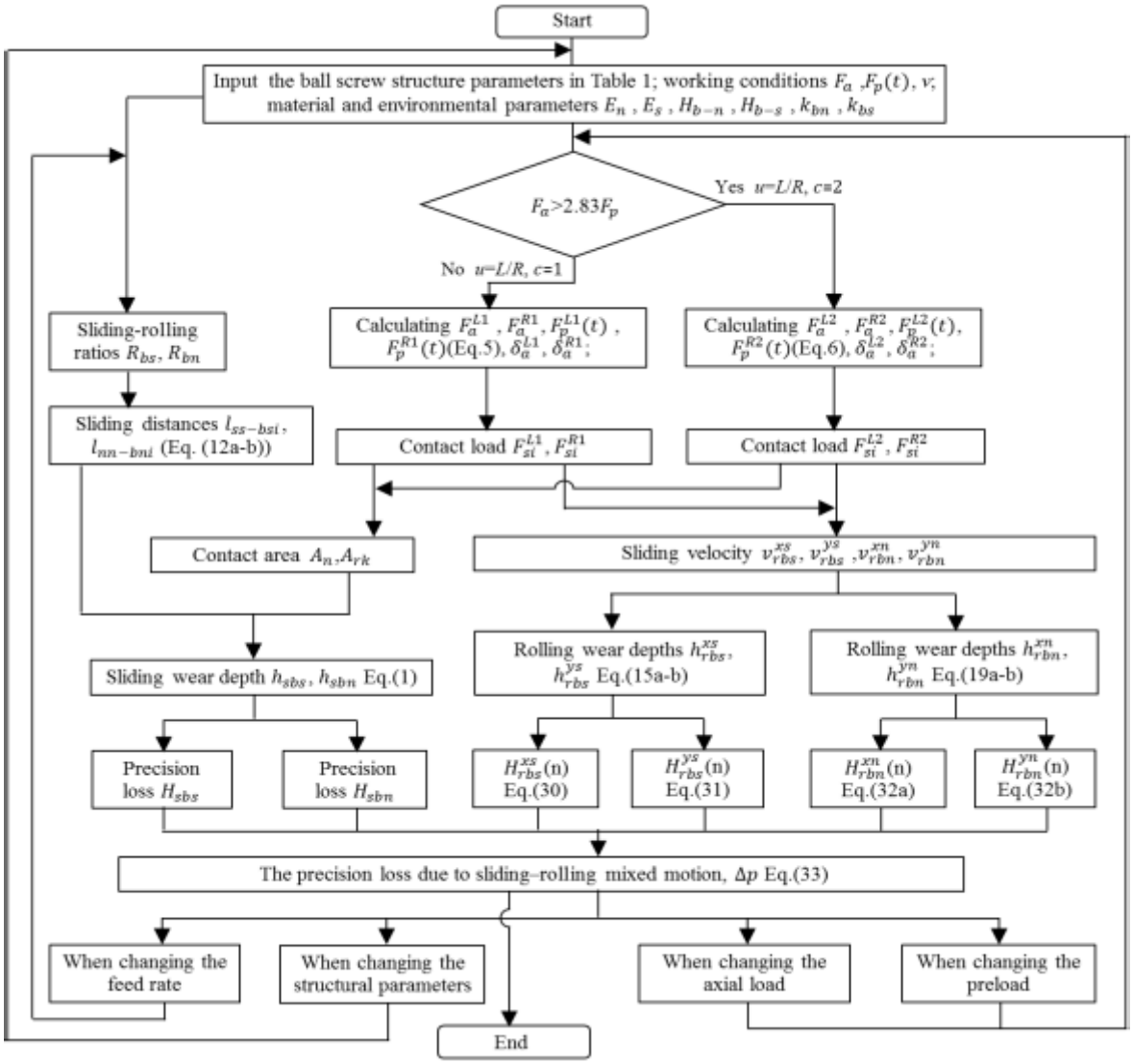

FIGURE 4. **Flow chart of precision loss calculation.**

using the models of Wei and Lai [4], Zhou *et al.* [11], and Liu *et al.* [12].

Fig. 6(a) shows the variation of cumulative BSM rolling motion wear obtained by combining Eq. (30) and (31). Similarly, according to Eq. 32(a) and (b), the rolling motion wear depth for effective transmission between the ball and nut in the x_n and y_n directions can be obtained. The variation of wear depth is shown in Fig. 6(b).

Before the test, V_μ^0 was measured as the initial value. Then V_μ^t was measured once every 50 h. The test was repeated 5 times and the average V_μ^t was calculated. The precision loss was calculated at each time point as the difference between V_μ^0 and V_μ^t. To verify the precision loss model of the ball screw under mixed sliding-rolling motion, a test platform was established. Precision losses were measured after the BSM reached stable operating conditions. Fig. 7 illustrates

$$h_{rbs}^{xs}(n) = \frac{n_{xs}k_{bs}a_{xs}F_{si}^{uc}\zeta_{xs}\left\{r\left(\delta_a^{uc}-r\right)\left(\omega_n\cos\theta_{si}^{uc}+\omega_b\sin\theta_{si}^{uc}\right)+\omega rR_{bs}\left[\left(r-\delta_a^{uc}\right)\cos\theta_{si}^{uc}-R\right]\right\}}{4c_{xs}a_{ys}} \tag{24}$$

$$h_{rbn}^{xn}(n) = \frac{n_{xn}k_{bn}a_{xn}F_{ni}^{uc}\zeta_{xn}r\left\{\left(\delta_a^{uc}-r\right)\left(\omega_n\cos\theta_{ni}^{uc}+\omega_b\sin\theta_{ni}^{uc}\right)-\omega_N R_{bn}\left[R+\left(r-\delta_a^{uc}\right)\cos\theta_{ni}^{uc}\right]\right\}}{4c_{xn}a_{yn}} \tag{28}$$

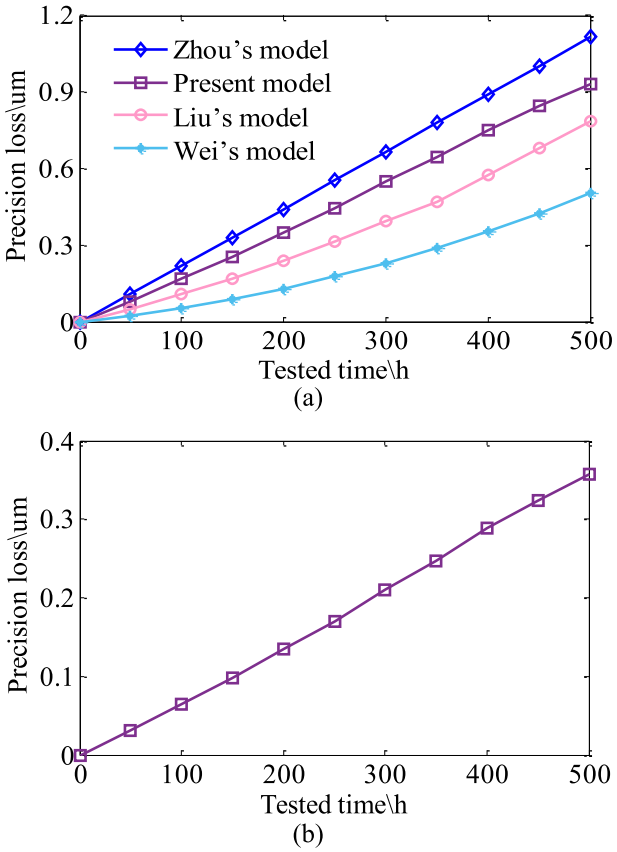

FIGURE 5. BSM precision loss due to sliding motion wear: (a) between ball and screw, (b) between ball and nut.

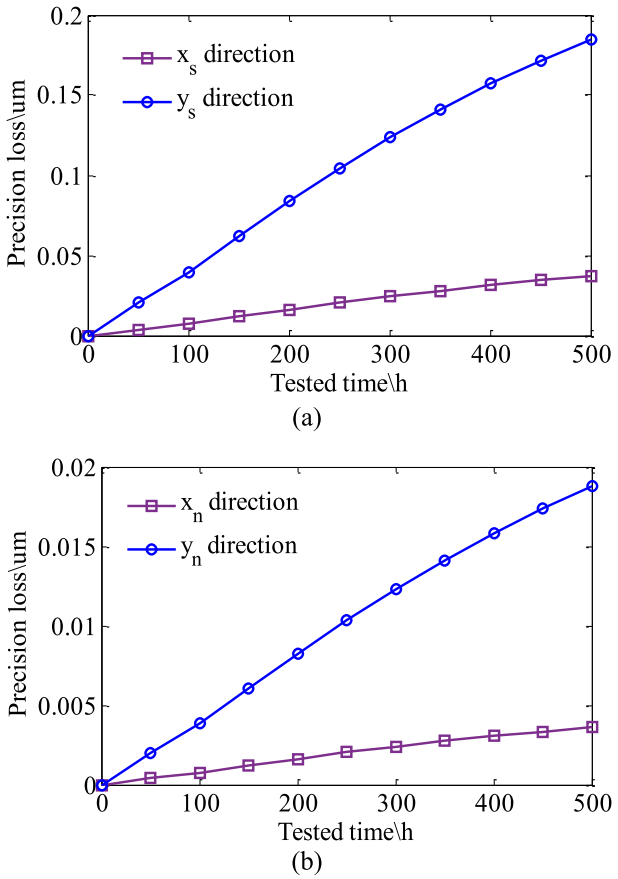

FIGURE 6. BSM precision loss due to rolling motion wear: (a) Precision loss due to rolling motion wear between the ball and the screw; (b) Precision loss due to rolling motion wear between the ball and the nut.

the method used to measure the precision loss using a laser interferometer (XD Dual Frequency Laser Interferometer). The laser signal was used as the reference length to accurately measure the positional accuracy and geometric accuracy of the numerical control equipment.

The experiment was carried out as follows: (1) The initial positioning error of the ball screw was measured with V_μ as the precision loss index; (2) The required test parameters were set according to the initial working conditions defined in Section 3.2 (F_p = 1330 N, F_a = 2500 N, v = 240 mm/min, grease lubrication (KOC301), ambient temperature of 23°C); (3) The positioning error of the ball screw was measured every 50 h using a laser interferometer; (4) Data on positioning error after wear and initial positioning error were processed and analyzed to obtain precision loss values. The total test time was 500 h.

Fig. 8 shows the platform for testing BSM precision loss. The axial load and feed rate were set according to the test requirements. Flow and pressure of the hydraulic oil were controlled by the load center using the servo valve. Hydraulic oil enters the loading cylinder through the pressure input and flows back to the loading center through the pressure output. For axial loading, a preset pressure is applied to the working nut. The feed rate is programmed and set to the desired experimental working conditions.

The operating principle of the feed rate is that by controlling the operation of the center platform, the feed rate can be programmed and realized according to the experimental working conditions.

Combining Eqs. (22) and (23) with Eqs. (30)–(33), the precision loss due to mixed sliding-rolling motion was obtained. The results are presented in Fig. 9.

Combining the results presented in Fig. 5 and 6 with those in Fig. 9, it can be concluded that the BSM precision loss due to mixed sliding-rolling motion behavior can be used to predict the precision loss rate under certain operation conditions and rolling motion. The precision loss due to rolling motion between the ball and raceway is responsible for 29.09% of the screw precision loss due to sliding motion. Additionally, the total precision loss due to rolling motion accounts for 21.03% of the total sliding wear depth of the screw and nut and 17.38% of the overall BSM precision loss under mixed sliding-rolling motion. Therefore, precision degradation due to rolling motion influences the total precision loss of the BSM and should be considered.

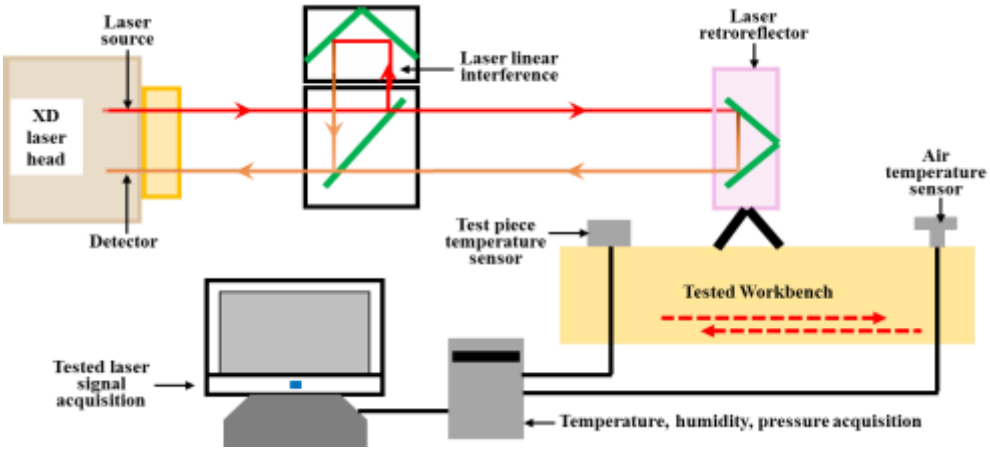

FIGURE 7. Method used for measuring BSM precision loss using laser interferometer.

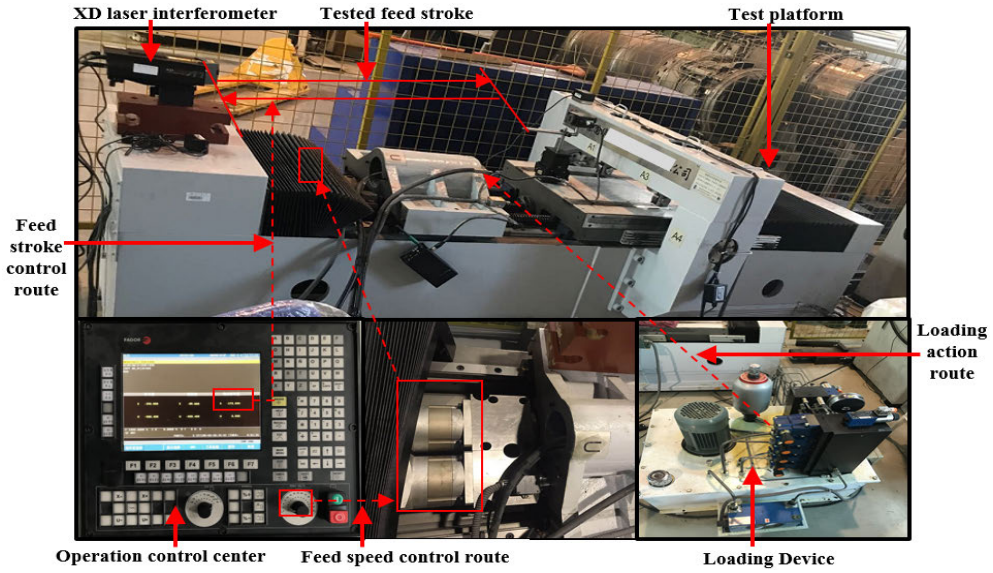

FIGURE 8. Test platform for measuring BSM precision loss due to sliding-rolling mixed motion behavior.

According to Fig. 9, effectiveness of the accuracy loss model can be measured by calculating the absolute error and relative error between the theoretical and the experimental values, as shown in Table 2.

The results indicate that the ball screw is in a stable wear stage from 0–500 h. The maximum absolute error between the theoretical precision loss and the experimental value is 0.139 μm. The average absolute error is 0.0525 μm, the maximum relative error is 15.30%, and the average relative error is 7.93%. The results show that the precision loss model has higher accuracy when mixed sliding-rolling motion is considered.

C. FACTORS INFLUENCING PRECISION LOSS

According to the precision loss analysis, when lubrication grease is used, factors influencing precision loss include operating conditions, such as contact load (F_{si}^{uc}, F_{ni}^{uc}) and feed rate ($v = \omega L_S$), as well as structural parameters, such as contact angle (θ_{si}^{uc}, θ_{ni}^{uc}), helix angle (α), nominal diameter ($D = 2R$), and ball diameter ($D_b = 2r$). For a double-nut ball screw, the contact load is related to the axial load (F_a) and preload (F_p). According to the flowchart shown in Fig. 4,

$$\Delta p = f\left(F_p, F_a, v, \theta_k, \alpha, D, D_b\right) \tag{34}$$

where ω is the rotating speed of screw and L_S is the lead. θ_{si}^{uc}, θ_{ni}^{uc} are the actual contact angle considering contact deformation between ball and raceway: $\theta_{si}^{L1} = \theta_{ni}^{L1} = \theta_{L1} + \theta'_{L1}$, $\theta_{si}^{R1} = \theta_{ni}^{R1} = \theta_{R1} + \theta'_{R1}$, $\theta_{si}^{L2} = \theta_{ni}^{L2} = \theta_{L2} + \theta'_{L2}$, $\theta_{si}^{R2} = \theta_{ni}^{R2} = \theta_{R2} + \theta'_{R2}$. Furthermore, θ_{L1}, θ_{R1}, θ_{L2} and θ_{R2} describe the initial contact angles before contact deformation: $\theta_k = \theta_{L1} = \theta_{R1} = \theta_{L2} = \theta_{R2}$.

Results of the precision loss analysis and ball screw experiment (Section 3.2) suggest higher accuracy of the precision loss model when mixed sliding-rolling motion is considered. Taking the initial working conditions of Section 3.2 and the ball screw structural parameters in Table 1 as an example, the effects of preload, axial load, and feed rate of the screw on the precision loss were investigated. The influence of preload,

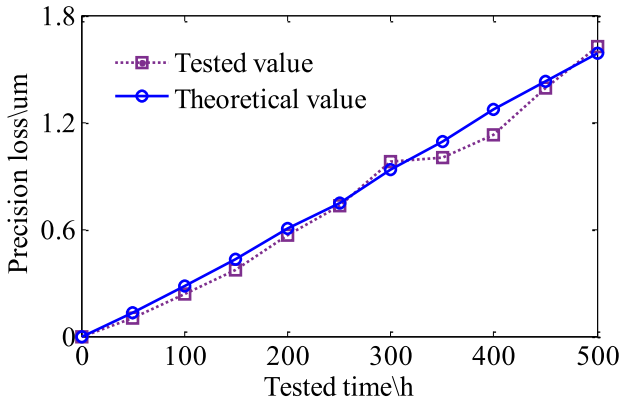

FIGURE 9. BSM precision loss due to sliding-rolling mixed motion behavior.

TABLE 2. Precision loss analysis.

Time (h)	Theoretical precision loss (μm)	Experimental precision loss (μm)	Absolute error (μm)	Relative error (%)
0	0	0	0	/
50	0.131	0.115	-0.016	-12.21
100	0.281	0.238	-0.043	-15.30
150	0.432	0.371	-0.061	-14.12
200	0.604	0.566	-0.038	-6.29
250	0.753	0.735	-0.018	-2.39
300	0.936	0.985	0.049	5.24
350	1.097	1.008	-0.089	-8.11
400	1.273	1.134	0.139	-10.92
450	1.436	1.401	-0.035	-2.44
500	1.596	1.633	0.037	2.32

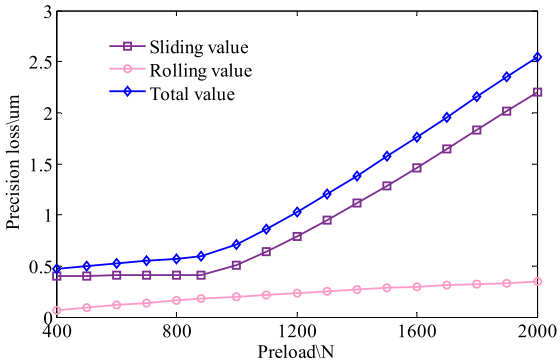

FIGURE 10. Effect of preload on precision loss under mixed sliding-rolling motion.

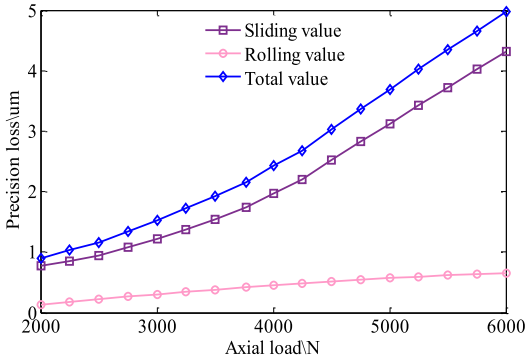

FIGURE 11. Effect of axial load on precision loss under mixed sliding-rolling motion.

axial load, and feed rate on the precision loss when all other operating conditions were held constant are illustrated in Figs. 10–12.

When the axial load is 2500 N, as the preload increases, the ball in the right nut appears to be unloaded. According to Eq. (6), the contact load is zero when the preload is 883.4 N. When 400 N $< F_p(t) <$ 883.4 N, the precision loss between the screw and the ball in the left nut increases slowly and the precision loss between the screw and the ball in the right nut decreases slowly. In this case, the contact load between the ball in the left nut and the raceway gradually increases and the contact load between the ball in the right nut and the raceway gradually decreases.

When 2000 N $> F_p(t) >$ 883.4 N, the precision loss between the balls of the right and left nuts and the raceways (screw raceway, nut raceway) increase since, according to Eq. (5), the contact load gradually increases as the preload increases; Therefore, in Fig. 10, as the preload increases, the precision loss of the ball screw increases under both sliding and rolling motion. Since the preload increases, the contact load also increases, thus, the amount of wear increases resulting in greater precision loss.

When the preload is 1330 N, the ball in the right nut appears to be unloaded as the axial load increases. According to Eq. (6), the contact load is zero when the axial load is 3763.9 N. When 2000 N $< F_a <$ 3763.9 N, the precision loss between the screw and the ball in the left nut increases slowly and the precision loss between the screw and the ball in the right nut decreases slowly. This is because the contact load between the ball in the left nut and the raceway gradually increases and the contact load between the ball in the right nut and the raceway gradually decreases. In this case, total precision loss between the ball and the raceway increases slowly.

When 6000 N $> F_a >$ 3763.9 N, precision losses between the balls of the left and right nuts and the raceways increase since, according to Eq. (5), the contact load gradually increases as the axial load increases; Therefore, in Fig. 11, the precision loss of the ball screw increases under both sliding motion and rolling motion as the preload increases. When the axial load is increased, the contact load also increases, thus, the amount of wear increases resulting in greater precision loss.

In Fig. 12, as the feed rate increases, both the precision loss between the ball and the screw raceway and the precision loss between the ball and the nut raceway increase, because the sliding velocity and sliding distance increase as the feed rate increases, resulting in faster precision loss.

Similarly, the precision loss model presented in Section 3.2 was used to study the influence of structural parameters on the ball screw precision loss. The effects of contact angle, helix

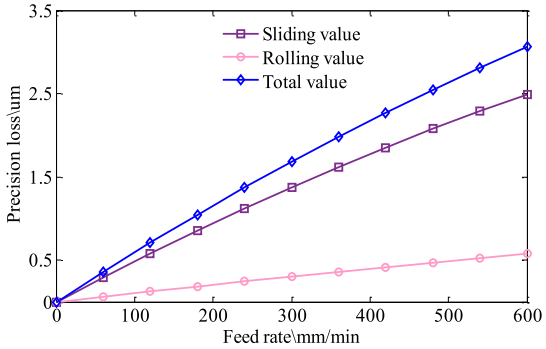

FIGURE 12. Effect of feed rate on precision loss under mixed sliding-rolling motion.

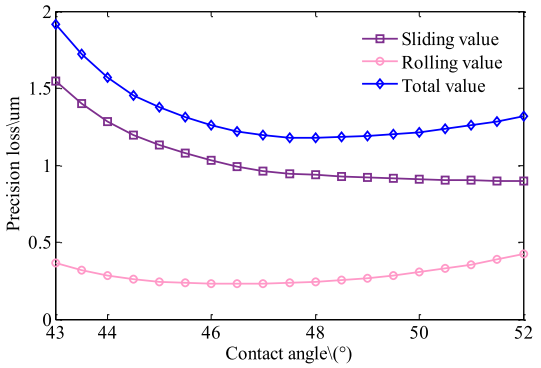

FIGURE 13. Effect of contact angle on precision loss under mixed sliding-rolling motion.

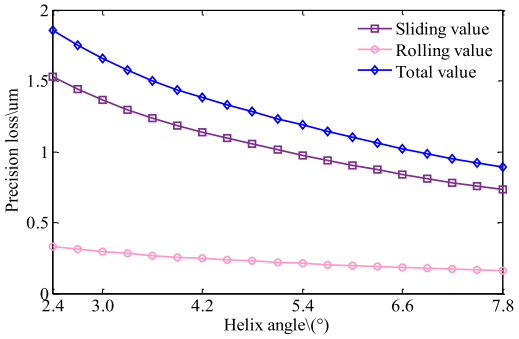

FIGURE 14. Effect of helix angle on precision loss under mixed sliding-rolling motion.

angle, nominal diameter, and ball diameter were examined, as shown in Figs. 13–16.

In Fig. 13, although the precision loss value gradually decreases under sliding motion, the precision loss under rolling motion tends to decrease first and then increase. Therefore, the ball screw precision loss exhibits the phenomenon of first decreasing and then gradually increasing.

Fig. 14 shows that the precision loss under both sliding motion (between the ball and left and right nut and between the screw and ball in the left and right nut) and rolling motion (between the ball and left and right nut and between the screw

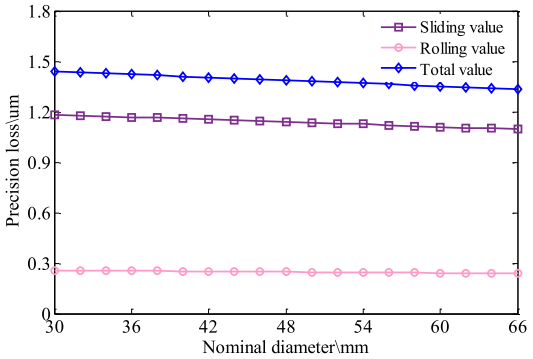

FIGURE 15. Effect of screw nominal diameter on precision loss under mixed sliding-rolling motion.

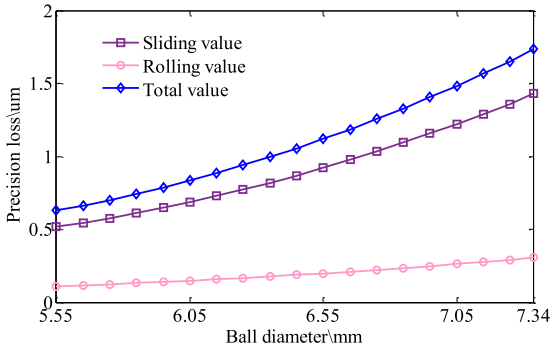

FIGURE 16. Effect of ball diameter on precision loss under mixed sliding-rolling motion.

and ball in the left and right nut) decrease as the helix angle increases. Since feed rate is constant, the rotational velocity (w) of the screw can be reduced by increasing the helix angle; therefore, the relative sliding velocity and sliding distance between the ball and the raceway decrease and accuracy loss decreases.

Fig. 15 shows that as the nominal diameter of the screw increases, the precision loss under sliding motion (between the ball and the left and right nut and between the screw and the ball in the left and right nut) and the precision loss under rolling action exhibit only a small decrease; Therefore, the nominal diameter of the screw has very little effect on the precision loss of the ball screw compared to contact angle and helix angle.

Fig. 16 shows that the precision loss under sliding motion (between the ball and the left and right nut and between the screw and the ball in the left and right nut) and rolling action increase as the ball diameter increases.

The sum of the squared difference between the precision loss and the initial precision loss for influencing factor q is denoted $\sum \left(p_{qi} - \overline{p_{qs}}\right)^2$. The sensitivity of precision loss to influencing factor q can be expressed as

$$S_q = \sqrt{\frac{\sum_{i=1}^{N_q} \left(p_{qi} - \overline{p_{qs}}\right)^2}{N_q \overline{p_{qs}} \left|\Delta p_{if}\right|}} \tag{35}$$

TABLE 3. The structural sensitivity parameter.

Classification name	N_q	$\overline{p_{qs}}$	Δp_{if}	$\sum(p_{qi}-\overline{p_{qs}})^2$
Contact angle	37	1.374	9	1.384370
Helix angle	37	1.374	5.4	3.155076
Nominal diameter	37	1.374	36	0.041799
Ball diameter	37	1.374	1.8	5.946009
Preload	37	1.374	1600	18.669669
Axial load	37	1.374	4000	121.664366

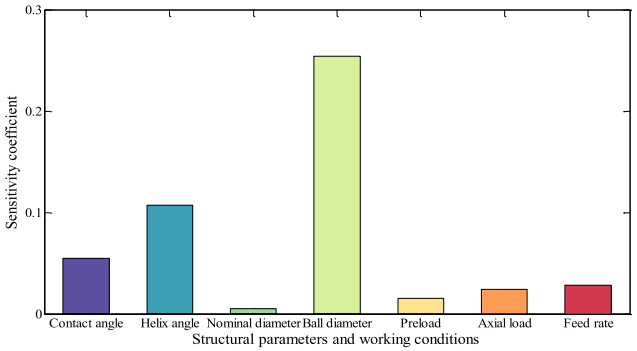

FIGURE 17. Sensitivity coefficient for precision loss.

where p_{qi} is precision loss of the ith sample for influencing factor q; $\overline{p_{qs}}$ represents the precision loss of the ball screw under a given set of working conditions and the initial structural parameters; N_q is the total number accuracy loss measurements for influencing factor q; $|\Delta p_{if}|$ is the absolute value of influencing factor q. Each parameter was calculated separately, as shown in Table 3.

Eq. (35) was used to analyze the sensitivity of precision loss to structural parameters and working conditions, as shown in Fig.17.

From Fig. 17, the sensitivity coefficients of the structural parameters, including contact angle, helix angle, nominal diameter, and ball diameter, are 0.0550061, 0.107205, 0.00477899, and 0.254907, respectively. The sensitivity coefficients of the working conditions, including preload, axial load, and feed rate are 0.0151501, 0.0244601 and 0.0280608, respectively. With the exception of nominal diameter, the sensitivity coefficient of other structural parameters to precision loss is greater than those of the working conditions. Thus, the influence of the structural parameters on precision loss (with the exception of nominal diameter) is greater than those of the working conditions. Nominal diameter has the weakest influence on precision loss, compared with both other structural parameters and working conditions; therefore, ball diameter, contact angle, and helix were determined to be the most important structural parameters influencing precision loss.

IV. OBJECTIVE FUNCTION FOR OPTIMIZATION OF PRECISION RETENTION

A. OPTIMIZATION MODEL FOR PRECISION RETENTION

Based on the precision loss model, an optimization model for ball screw precision retention was developed. According to the results presented in Section 3.2, the axial load, preload, and feed rate are the main factors influencing the precision loss of the BSM. In addition, the main structural parameters affecting precision loss are contact angle, helix angle, and ball diameter. By optimizing the structural parameters, the precision retention of the ball screw can be improved under certain operating conditions. Taking the contact angle, helix angle, and ball diameter as the optimization parameters,

$$X = [\theta_k, \alpha, D_b]^T = [x_1, x_2, x_3]^T \tag{36}$$

Decreasing the precision loss rate can improve the precision retention of the ball screw. According to Eq. (34), minimizing the precision loss can improve the precision retention of the ball screw. Thus, the target expression for the optimization analysis can be written as

In Eq. (37), as shown at the bottom of the next page, t_b is the raceway curvature ratio, which is in the range 1.04 to 1.11. At the end of the calculation, $t_b = 1.09$. The Hertzian contact ellipse parameter N_H can be obtained as [25]

$$N_H^{\frac{2}{3}} = \sqrt[3]{1.0339}\left(\sum \rho_1 / \sum \rho_2\right)^{0.212} \times \left(1.0003 + 0.5968\left(\sum \rho_1 / \sum \rho_2\right)\right) \tag{38}$$

Then, when the ball is in contact with the screw:

$$\sum \rho_1 = \frac{2}{x_3} + \frac{2\cos x_1 \cos x_2}{2R - x_3 \cos x_1}, \quad \sum \rho_2 = \frac{2}{x_3} - \frac{2}{1.09 x_3} \tag{39}$$

When the ball is in contact with the nut raceway:

$$\sum \rho_1 = \frac{2}{x_3} - \frac{2\cos x_1 \cos x_2}{x_3 + x_3 \cos x_1}, \quad \sum \rho_2 = \frac{2}{x_3} - \frac{2}{1.09 x_3} \tag{40}$$

B. CONSTRAINTS OF OPTIMIZATION MODEL

It is necessary to consider performance constraints and geometric constraints in the optimization process. Performance constraints of the ball screw include the transmission efficiency and dynamic load, and geometric constraints are contact angle, helix angle, ball diameter, etc. The transmission efficiency of the ball screw must be greater than 90%. After applying a preload, the transmission efficiency can be expressed as [3]

$$\eta_p = \eta \Big/ \left[1 + \frac{1}{\varepsilon}\left(1 - \eta^2\right)\right] \tag{41}$$

where ε is the ratio of axial load to preload and η is the transmission efficiency without the preload. The transmission efficiency can be calculated as

$$\eta = \tan\alpha / \tan(\alpha + \lambda) \tag{42}$$

In Eq. (42), λ is the equivalent friction angle, calculated by

$$\lambda = \tan^{-1}[0.01/r \sin\alpha] \tag{43}$$

Combining Eqs. (42) and (43), the transmission efficiency constraint can be written as

$$C_1(X) = 0.9 - \eta \Big/ \left[1 + \frac{1}{\varepsilon}\left(1 - \eta^2\right)\right] \le 0 \tag{44}$$

The rated dynamic load of the ball screw is [27], [28], (45) as shown at the bottom of the next page.

The condition for meeting the dynamic load constraint of the ball screw can be written as

$$C_2(X) = C_{d0} - [C_{d0}] \le 0 \tag{46}$$

The contact angle constraints are [20], [22], [29]

$$C_3(X) = 43 - x_1 \le 0 \tag{47a}$$
$$C_4(X) = x_1 - 52 \le 0 \tag{47b}$$

The helix angle constraints can be written as [8], [29], [30]

$$C_5(X) = 2.73 - x_2 \le 0 \tag{48a}$$
$$C_6(X) = x_2 - 7 \le 0 \tag{48b}$$

According to the range of the raceway curvature ratio values, $1.04 \le t_b \le 1.11$ [29], the ball diameter constraints can be expressed as

$$C_7(X) = 6.618 - x_3 \le 0 \tag{49a}$$
$$C_8(X) = x_3 - 7.063 \le 0 \tag{49b}$$

V. STRUCTURAL PARAMETER OPTIMIZATION AND APPLICATION

A. STRUCTURE OPTIMIZATION FOR PRECISION RETENTION

Based on the precision loss calculation and parameter analysis, an optimization target was established and the optimization constraints were set. According to Sections 4.1 and 4.2, the optimization model for ball screw precision retention considering the effects of mixed sliding-rolling motion can be expressed as

$$\begin{cases} \min\ \Delta p \\ s.t.\ C_i(X) \le 0, \quad i = 1, 2, \ldots, 8 \\ X = [x_1, x_2, x_3]^T = [\theta_k, \alpha, D_b]^T \end{cases} \tag{50}$$

There is a nonlinear relationship between structural parameters of the ball screw and precision retention. Neural fuzzy control theory (NFCT) can be used to solve this type of nonlinear problem [31]. However, the advanced neural fuzzy network (ANFN) has higher computational accuracy than the NFCT [32], [33] and was adopted in this article, as shown in Fig. 18.

Steps of the structure optimization based on the ANFN are:

(1) In the first layer of the premise network, the structural parameters are connected one by one to each solid black spot. The purpose of layer 1 is to transfer the structural parameter variables to layer 2. The number of variables in the first layer is n.

(2) In layer 2, each lingual variable is individually associated with a solid black spot. The membership grade of each component belonging to each linguistic variable is calculated: $g_k^c = g_{L_k^c}(x_k)$, $(k = 1, 2, \ldots, n; c = 1, 2, \ldots, \mu_k)$. Then, the membership function of the fuzzy set of linguistic structural parameter variables is obtained using the sigmoid function: $f(x, b, z) = \left(1 + e^{-b(x-z)}\right)^{-1}$. The number of variables in the layer is $\sum_{k=1}^{n} \mu_k$.

(3) In layer 3, the fitness of each linguistic structural parameter variable is calculated based on fuzzy rules: $s_c = \min\left\{g_1^{i_1}, g_2^{i_2}, \ldots, g_n^{i_n}\right\}$, $i_1 \in \{1, 2, \ldots, \mu_1\}$; $i_2 \in \{1, 2, \ldots, \mu_2\}$; $\ldots$; $i_n \in \{1, 2, \ldots, \mu_n\}$, $c = 1, 2 \ldots, \mu$.

(4) In layer 4, the overall fitness of the linguistic structural parameter variables is calculated: $\overline{S_c} = \frac{s_c}{\sum_{c=1}^{\mu} s_c}$, $c = 1, 2 \ldots, \mu$.

(5) In the latter network, layer 1 is an input layer. The rule for each solid black spot in layer 2 is $w_{1c} = d_{c0} + d_{c1}x_1 + d_{c2}x_2 + \ldots + d_{cn}x_n = \sum_{k=0}^{n} d_{ck}x_k (c = 1, 2, \ldots, \mu)$ where d_{ck} $(c = 1, 2, \ldots, \mu; k = 1, 2, \ldots, n)$ is the connection weight. The purpose of layer 3 is to obtain the output: $q_z = \sum_{c=1}^{\mu} \overline{S_c} d_{1c}$.

(6) The corrective network is used to correct the membership function and to share the operating rules with the premise network. The membership function of the fuzzy set of linguistic structural parameter variables in layer 2 is $f_i(x, b_l, z_l) = \left(1 + e^{-b_l(x-z_l)}\right)^{-1}$, where d_l and z_l are the coefficients of the membership function.

$$\Delta p = \frac{\cos x_2}{\sin x_1}\left\{\int_0^{L_{b-s}}\left[\frac{C_{b-s}Mk_{bs}L_{bsi}\sqrt[3]{F_{si}^{uc}}E^{*\frac{2}{3}}}{\sqrt[3]{36\pi}H_{b-s}i_t N_H^{\frac{2}{3}}\left(\frac{4}{x_3} - \frac{2}{t_b x_3} + \frac{2\cos x_1 \cos x_2}{2R - x_3\cos x_1}\right)^{2/3}} + \frac{n_{ys}k_{bs}F_{si}^{uc}a_{ys}\zeta_{ys}\left(\delta_a^{uc} - x_3\right)x_3\omega_t}{16c_{ys}a_{xs}} + \frac{n_{xs}k_{bs}a_{xs}F_{si}^{uc}\zeta_{xs}\left(\frac{x_3}{2} - \left(\delta_a^{uc} - \frac{x_3}{2}\right)(\omega_n\cos x_1 + \omega_b \sin x_1) + \omega R_{bs}\frac{x_3}{2}\left(\left(\frac{x_3}{2} - \delta_a^{uc}\right)\cos x_1 - R\right)\right)}{4c_{xs}a_{ys}}\right]dl\right.$$
$$\left. + \int_0^{L_{b-n}}\left[\frac{C_{b-n}Mk_{bn}L_{bni}\sqrt[3]{F_{ni}^{uc}}E^{*\frac{2}{3}}}{\sqrt[3]{36\pi}H_{b-n}i_t N_H^{\frac{2}{3}}\left(\frac{4}{x_3} - \frac{2}{t_b x_3} - \frac{2\cos x_1 \cos x_2}{2R + x_3\cos x_1}\right)^{2/3}} + \frac{n_{yn}k_{bn}F_{ni}^{uc}a_{yn}\zeta_{yn}\left(x_3 - \delta_a^{uc}\right)x_3\omega_t}{16c_{yn}a_{xn}} + \frac{n_{xn}k_{bn}a_{xn}F_{ni}^{uc}\zeta_{xn}\frac{x_3}{2}\left(\left(\delta_a^{uc} - \frac{x_3}{2}\right)(\omega_n\cos x_1 + \omega_b \sin x_1) - \omega_N R_{bn}\left(R + \left(\frac{x_3}{2} - \delta_a^{uc}\right)\cos x_1\right)\right)}{4c_{xn}a_{yn}}\right]dl\right\} \tag{37}$$

The square error of the output can be expressed as $\sum q_z = \left(q_z - q_z'\right)^2 \Big/ 2$ and the coefficients of the membership function are determined as follows:

$$\begin{cases} d_{ck}\,(m+1) = d_{ck}\,(m) - \xi \dfrac{\partial \sum q_z}{\partial d_{ck}} \\ \xi > 0 \\ c = 1, 2, \ldots, \mu \\ k = 1, 2, \ldots, n, \end{cases}$$

$$\begin{cases} b_{ki_k}\,(m+1) = b_{ki_k}\,(m) - \xi \dfrac{\partial \sum q_z}{\partial b_{ki_k}}; \\ \quad z_{ki_k}\,(m+1) = z_{ki_k}\,(m) - \xi \dfrac{\partial \sum q_z}{\partial z_{ki_k}} \\ b_{lki_k}\,(m+1) = b_{lki_k}\,(m) - \xi \dfrac{\partial \sum q_z}{\partial b_{lki_k}}; \\ \quad z_{lki_k}\,(m+1) = z_{lki_k}\,(m) - \xi \dfrac{\partial \sum q_z}{\partial z_{lki_k}} \\ k = 1, 2, \ldots, n \\ i_k = 1, 2, \ldots, \mu_k \end{cases}$$

When $\sum q_z\,(m) < \sum q_z\,(m)_{\min}$, the fitness value for precision loss was obtained, as shown in Fig. 19.

The structural parameters of the screw, including contact angle, helix angle, and ball diameter were optimized using the optimization model to improve the precision retention under the set of working conditions defined in Section 3.2. Optimized values of the contact angle, helix angle, and ball diameter are 49.57°, 5.86°, and 6.62 mm, respectively. The precision loss of the ball screw is 1.303 μm.

Compared with the precision loss before optimization of 1.596 μm, the optimization reduced the precision loss by 0.293 μm; Therefore, the reduction in precision loss rate is 18.36%. Thus, through the optimization analysis of the structural parameters, the precision retention of the ball screw was improved, which can extend the effective life of the ball screw.

Theoretical and experimental values of the precision loss of the ball screw under the original structural parameters were compared to the precision loss after the optimization, as shown in Fig. 20. The precision loss of the ball screw was reduced by varying degrees depending on the operating time. The experiment in Section 3 was extended to 800 hours, and the reduction in precision loss rate after optimization of the structural parameters of the ball screw were listed in Table 4. The rate of precision loss reduction was calculated as the reduced precision loss divided by the original precision loss value and adopted as the optimization index. A larger reduction in the precision loss rate indicates a greater optimization effect.

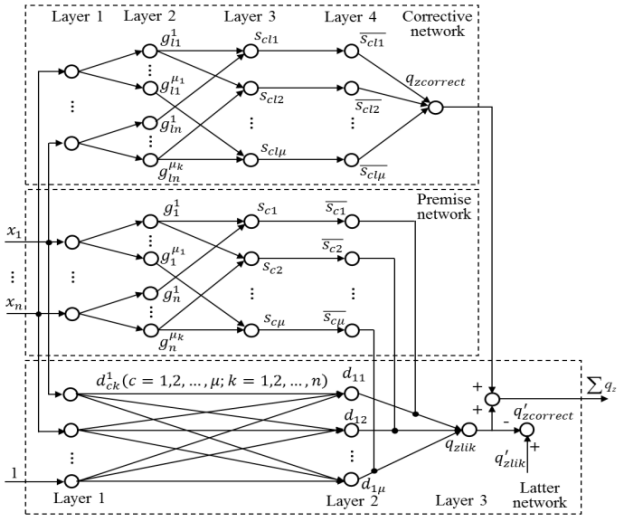

FIGURE 18. Structure optimization based on advanced neural fuzzy network (ANFN).

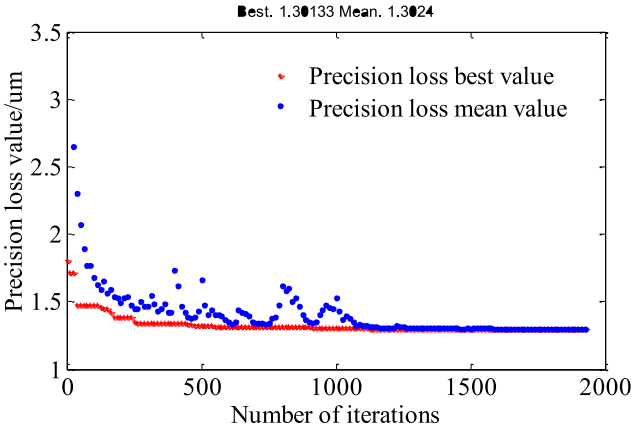

FIGURE 19. Results of ball screw optimization for precision retention.

In Table 4, The ITPLV means ''Initial theoretical precision loss value'', the IEPLV stands for ''Initial experimental precision loss value'', the OPLV is ''Optimized precision loss value'', the RPLRITV represents ''Reduction in precision loss relative to initial theoretical value'', the RPLRIEV means ''Reduction in precision loss relative to initial experimental value'', the RRRITV is ''Reduction rate relative to initial theoretical value'', the RRRIEV represents ''Reduction rate relative to initial experimental value''. From 0 to 750 h, the reduction in precision loss of the ball screw increased. The average reduction in the precision loss rate was approximately 19.02% compared to the initial theoretical value and approximately 13.98% compared to the initial experimental

$$[C_{d0}] = \frac{93.2\left(\frac{x_3}{2R}\cos x_1\right)^{0.3}\left(1-\frac{x_3}{2R}\cos x_1\right)^{1.39}\left(1-\frac{1}{3}\sin x_1\right)\tan x_1(\cos x_1)^{0.7}\left(\frac{2\pi R}{x_3}\right)^{2/3}x_3^{1.8}}{\left(1+\frac{x_3}{2R}\right)^{1/3}} \tag{45}$$

TABLE 4. Optimization analysis results under the working conditions defined in Section 3.2.

Time/h	ITPLV(μm)	IEPLV(μm)	OPLV(μm)	RPLRITV(μm)	RPLRIEV(μm)	RRRITV(%)	RRRIEV(%)
0	0	0	0	0	0	/	/
50	0.131	0.115	0.102	0.029	0.013	22.14	11.30
100	0.281	0.238	0.225	0.056	0.013	19.93	5.46
150	0.432	0.371	0.345	0.087	0.026	20.14	7.01
200	0.604	0.566	0.492	0.112	0.074	18.54	13.07
250	0.753	0.735	0.616	0.137	0.119	18.19	16.19
300	0.936	0.985	0.751	0.185	0.234	19.77	23.76
350	1.097	1.008	0.894	0.203	0.114	18.51	11.31
400	1.273	1.134	1.041	0.232	0.093	18.22	8.20
450	1.436	1.401	1.156	0.28	0.245	19.50	17.49
500	1.596	1.633	1.306	0.29	0.327	18.17	20.02
550	1.751	1.667	1.416	0.335	0.251	19.13	15.06
600	1.904	1.809	1.566	0.338	0.243	17.75	13.43
650	2.054	1.914	1.675	0.379	0.239	18.45	12.49
700	2.200	2.131	1.801	0.399	0.330	18.14	15.49
750	2.344	2.360	1.903	0.441	0.457	18.81	19.36
800	2.482	3.406	2.058	0.424	1.348	17.08	39.58

TABLE 5. Optimization analysis results under changing axial load conditions.

Time/h	ITPLV(μm)	IEPLV(μm)	OPLV(μm)	RPLRITV(μm)	RPLRIEV(μm)	RRRITV(%)	RRRIEV(%)
0	0	0	0	0	0	/	/
50	0.234	0.229	0.196	0.038	0.033	16.24	14.41
100	0.489	0.465	0.411	0.078	0.054	15.95	11.61
150	0.750	0.727	0.629	0.121	0.098	16.13	13.48
200	1.034	1.066	0.877	0.157	0.189	15.18	17.73
250	1.306	1.427	1.103	0.203	0.324	15.54	22.71
300	1.614	1.591	1.355	0.259	0.236	16.05	14.83
350	1.898	1.770	1.594	0.304	0.176	16.02	9.94
400	2.215	2.160	1.863	0.352	0.297	15.89	13.75
450	2.489	2.561	2.110	0.379	0.451	15.23	17.61
500	2.724	4.514	2.296	0.428	2.218	15.71	49.14

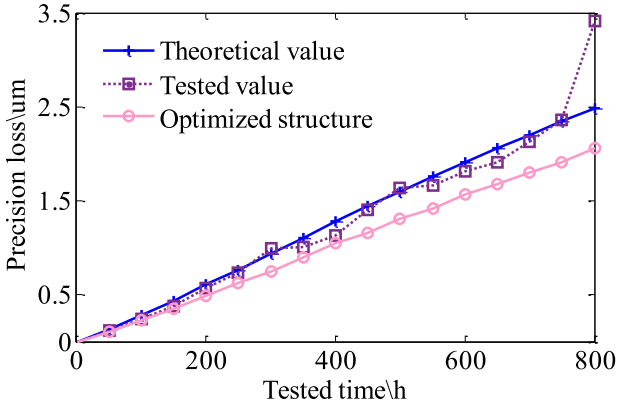

FIGURE 20. Comparison of precision loss before and after optimization.

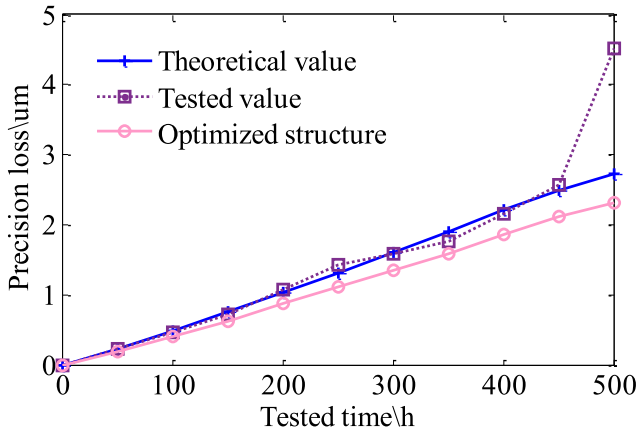

FIGURE 21. Comparison of precision retention before and after optimization.

value. Above 750 h, the optimized structural parameters are no longer valid for the ball screw precision loss model because severe wear of the ball screw will occur, thus, the precision loss can no longer be applied.

A precision loss value of 2.344 μm at 750 h was taken as the critical point for transition from stable wear to severe wear. For the optimized ball screw, the stable wear stage

was extended to 877 h, that is, by 127 h or 16.93%. Thus, based on our analysis, optimizing the structural parameters of the ball screw can reduce the precision loss. Furthermore, the precision retention can be improved, and optimization of the ball screw precision retention can be realized.

B. APPLICATION OF STRUCTURE OPTIMIZATION

To demonstrate the effectiveness of the optimized parameters, the precision retention of the ball screw was examined under different working conditions. The initial axial load F_a was set to 6000 N and all other working conditions were unchanged. The results are presented in Fig. 21.

When the axial load changes, the reduction in precision loss of the optimized ball screw varies at different time points. Precision loss reduction of the ball screw and reduction rate of precision loss are shown in Table 5.

From Table 5, the ball screw precision loss is reduced at different rates during different operating periods. From 0 to 450 h, the reduction in the precision loss of the ball screw increases. The average reduction in the precision loss rate is approximately 15.80% compared to the initial theoretical value and approximately 15.12% compared to the initial experimental value. For operating times greater than 450 h, the optimized structural parameters are no longer valid for the ball screw precision loss model since the ball screw is in the severe wear stage, thus, the precision loss model and optimized precision loss model cannot be applied. The precision loss of 2.344 μm at 429 h was taken as the critical point for transition from stable wear to severe wear. For the optimized ball screw, this time was extended to about 505h, that is, by 76 h or 17.72%.

When the axial load changes from 2500 N to 6000 N, the optimized structural parameters can still effectively ensure precision retention of the ball screw.

VI. CONCLUSION

In this article, an optimization analysis of structural parameters for precision retention of the ball screw was realized by considering mixed sliding-rolling motion. The results show that precision loss of the ball screw can be reduced to a certain extent, which can slow the rate of precision loss and the precision retention can be improved. In addition, when the axial load was varied, the optimal structural parameters still effectively ensured the precision retention. The main conclusions of this study can be summarized as follows:

(1) By optimizing the structural parameters of the ball screw under mixed sliding-rolling motion, the precision retention of the ball screw can be improved. In the theoretical analysis and experiment, grease lubrication (KOC301) was adopted, the preload was set to 1330 N, the axial load was 2500 N, the feed rate of screw was 240 mm/min, and the ambient temperature was 23°C. In the stable wear period, the average reduction in the precision loss rate of the ball screw was approximately 19.02% compared with the initial theoretical value and approximately 13.98% compared with the initial experimental value.

(2) When only the axial load varied from 2500 N to 6000 N and all other working conditions (lubrication method, preload, feed rate of screw, ambient temperature) remained the same, the stable wear stage was shorter. That is, the ability of the ball screw to maintain precision is degraded as the axial load increases. However, the precision retention of the ball screw can still be improved by optimizing the structural parameters. In the stable wear period, the average reduction in the precision loss rate of the ball screw is approximately 15.80% compared with the initial theoretical value and approximately 15.12% compared with the initial experimental value.

(3) Taking the precision loss of the ball screw in the transition stage from stable wear to the severe wear as the critical point, the stable wear stage can be extended by optimizing the structural parameters. When $F_a = 2500$ N, the stable wear phase can be extended from 750 h to 877 h, that is, by 127 h or 16.93%; When $F_a = 6000$ N, the stable wear phase can be extended from 429 h to 506 h, that is, by 76 h or 17.72%.

Based on the precision loss and parameter analysis, an optimized design of the ball screw for precision retention under mixed sliding-rolling motion was proposed. Depending on the feed rate, the optimization model can also improve the precision retention. Other applications of the optimization method will be considered in future research. In addition, other ball screw materials and different types of ball screws will be studied.

REFERENCES

[1] Y. Yong, Z. Wei-Min, Z. Qi-Xin, and J. Quan-Sheng, "Dynamic characteristic optimization of ball screw feed drive in machine tool based on modal extraction of state space model," *IEEE Access*, vol. 7, pp. 55524–55542, 2019.
[2] C. C. Wei and J. F. Lin, "Kinematic analysis of the ball screw mechanism considering variable contact angles and elastic deformations," *ASME J. Mech. Des.*, vol. 125, no. 4, pp. 33–717, 2003.
[3] M. C. Lin, S. A. Velinsky, and B. Ravani, "Design of the ball screw mechanism for optimal efficiency," *J. Mech. Des.*, vol. 116, no. 3, pp. 856–861, Sep. 1994.
[4] C.-C. Wei and R.-S. Lai, "Kinematical analyses and transmission efficiency of a preloaded ball screw operating at high rotational speeds," *Mechanism Mach. Theory*, vol. 46, no. 7, pp. 880–898, Jul. 2011.
[5] J. Zhao, M. Lin, X. Song, and Q. Guo, "Investigation of load distribution and deformations for ball screws with the effects of turning torque and geometric errors," *Mechanism Mach. Theory*, vol. 141, pp. 95–116, Nov. 2019.
[6] C. G. Zhou, H. T. Feng, and Z. T. Chen, "Correlation between preload and no-load drag torque of ball screws," *Int. J. Mach. Tool Manu.*, vol. 102, pp. 35–40, 2016.
[7] D. Olaru, G. C. Puiu, L. C. Balan, V. Puiu, T. D. In, and T. Roche, Eds., "A new model to estimate friction torque in a ball screw system," in *Product Engineering*. New York, NY, USA: Springer, 2004, pp. 333–346.
[8] N. Xu, W. Tang, Y. Chen, D. Bao, and Y. Guo, "Modeling analysis and experimental study for the friction of a ball screw," *Mechanism Mach. Theory*, vol. 87, pp. 57–69, May 2015.
[9] J. F. Archard, "Contact and rubbing of flat surfaces," *J. Appl. Phys.*, vol. 24, no. 8, pp. 981–988, Aug. 1953.
[10] C.-C. Wei, W.-L. Liou, and R.-S. Lai, "Wear analysis of the offset type preloaded ball–screw operating at high speed," *Wear*, vols. 292–293, pp. 111–123, Jul. 2012.

[11] C.-G. Zhou, Y. Ou, H.-T. Feng, and Z.-T. Chen, "Investigation of the precision loss for ball screw raceway based on the modified archard theory," *Ind. Lubrication Tribol.*, vol. 69, no. 2, pp. 166–173, Mar. 2017.

[12] J. Liu, C. Ma, and S. Wang, "Precision loss modeling method of ball screw pair," *Mech. Syst. Signal Process.*, vol. 135, Jan. 2020, Art. no. 106397.

[13] Q. Cheng, B. Qi, Z. Liu, C. Zhang, and D. Xue, "An accuracy degradation analysis of ball screw mechanism considering time-varying motion and loading working conditions," *Mechanism Mach. Theory*, vol. 134, pp. 1–23, Apr. 2019.

[14] F. Zhang, J. Huang, F. Chu, and L. Cui, "Mechanism and method for outer raceway defect localization of ball bearings," *IEEE Access*, vol. 8, pp. 4351–4360, 2020.

[15] C. E. Okwudire, "Improved Screw–Nut interface model for high-performance ball screw drives," *J. Mech. Design*, vol. 133, no. 4, Apr. 2011, Art. no. 041009.

[16] R. Caracciolo and D. Richiedei, "Optimal design of ball-screw driven servomechanisms through an integrated mechatronic approach," *Mechatronics*, vol. 24, no. 7, pp. 819–832, Oct. 2014.

[17] Q. Wang and M. Lin, "Design of new giant magnetostrictive structures for double-nut ball screw pre-tightening," *J. Brazilian Soc. Mech. Sci. Eng.*, vol. 39, no. 8, pp. 3181–3188, Aug. 2017.

[18] Z.-H. Zhao, Y.-L. Guan, and S.-A. Chen, "Experimental research on PMSM ball screw actuator and structural design suggestion of featured active suspension," *IEEE Access*, vol. 8, pp. 66163–66177, 2020.

[19] N. Riaz, S. I. A. Shah, F. Rehman, S. O. Gilani, and E. Udin, "A novel 2-D current signal-based residual learning with optimized softmax to identify faults in ball screw actuators," *IEEE Access*, vol. 8, pp. 115299–115313, 2020.

[20] T. Miura, A. Matsubara, D. Kono, K. Otaka, and K. Hoshide, "Design of high-precision ball screw based on small-ball concept," *Precis. Eng.*, vol. 47, pp. 452–458, Jan. 2017.

[21] K. Chen, L. Zu, and L. Wang, "Prediction of preload attenuation of ball screw based on support vector machine," *Adv. Mech. Eng.*, vol. 10, no. 9, 2018, Art. no. 1687814018799161.

[22] J. Hu, M. Wang, and T. Zan, "The kinematics of ball-screw mechanisms via the slide–roll ratio," *Mechanism Mach. Theory*, vol. 79, pp. 158–172, Sep. 2014.

[23] J. J. Kalker and K. L. Johnson, "Three-dimensional elastic bodies in rolling contact," *J. Appl. Mech.-Trans. ASME*, vol. 60, no. 1, pp. 34–45, 1993.

[24] L. Rodríguez-Tembleque, R. Abascal, and M. H. Aliabadi, "A boundary element formulation for wear modeling on 3D contact and rolling-contact problems," *Int. J. Solids Struct.*, vol. 47, nos. 18–19, pp. 2600–2612, Sep. 2010.

[25] T. A. Harris, *Rolling Bearing Analysis*. New York, NY, USA: Wiley, 2001.

[26] B. J. Hamrock and D. Dowson, *Ball Bearing Lubrication: The Elastohydrodynamics of Elliptical Contacts*. New York, NY, USA: Wiley, 1981.

[27] H. Hertz, "The contact of elastic solids," *J. Reine. Angew. Math.*, vol. 92, pp. 71–156, 1881.

[28] *Ball Screws—Part 5: Static and Dynamic Axial Load Ratings and Operational Life*, Standard 3408-5:2006, 2011.

[29] G. G. Cheng, Z. K. Shi, and C. P. Zhang, *Design of Ball Screw*, 4th ed. Beijing, China: China Machine Press, 1987.

[30] C. C. Wei, J. F. Lin, and J.-H. Horng, "Analysis of a ball screw with a preload and lubrication," *Tribol. Int.*, vol. 42, nos. 11–12, pp. 1816–1831, Dec. 2009.

[31] P. N. Koustoumpardis and N. A. Aspragathos, "Intelligent hierarchical robot control for sewing fabrics," *Robot. Comput.-Integr. Manuf.*, vol. 30, no. 1, pp. 34–46, Feb. 2014.

[32] Y. Zhang, "Improved TS fuzzy neural network applied in soft sensing of chemical industry," *J. Electron. Meas. Instrum.*, vol. 24, no. 6, pp. 585–589, 2010.

[33] Z. Zhang, Y. Qi, and Q. Cheng, "Machining accuracy reliability during the peripheral milling process of thin-walled components," *Robot. Cim-Int. Manuf.*, vol. 59, pp. 222–234, 2019.

BAOBAO QI received the B.S. degree in vehicle engineering from Anhui Science and Technology University, in 2015, and the M.S. degree in mechanical engineering from the Beijing University of Technology, in 2018, where he is currently pursuing the Ph.D. degree in mechanical engineering.

His research interests include accuracy degradation of CNC machine tool transmission components under time-varying conditions, and optimized design for precision retention.

QIANG CHENG received the Ph.D. degree in industrial engineering from the Huazhong University of Science and Technology, in 2009.

He is currently a Professor with the College of Mechanical and Electrical Engineering, Beijing University of Technology, China. His research interests include reliability design and precision retention design of CNC machine tool, state monitoring technology for high-end manufacturing equipment, and intelligent manufacturing production line planning.

ZHIFENG LIU received the Ph.D. degree in mechanical design from the Mechanical Engineering and Automation College, Northeastern University, in 2001.

He is currently the Associate Dean of the College of Mechanical Engineering and Applied Electronics Technology, Beijing University of Technology, where he is also the Director of the Beijing Key Laboratory of Advanced Manufacturing Technology. His research interests include digital design and manufacturing, manufacturing services, and manufacturing system information.

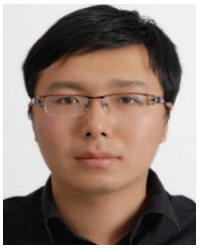

CONGBIN YANG received the Ph.D. degree in man machine and environmental engineering from the Beijing Institute of Technology, in 2015.

He is currently a Research Fellow with the Beijing Key Laboratory of Advanced Manufacturing Technology, Beijing University of Technology. He has hosted and participated on multiple research projects over the past three years. His research interests include control technology for tracked vehicles and structural dynamic coupling properties, and intelligent manufacturing.